Attention Mechanisms Don't Learn Additive Models: Rethinking Feature Importance for Transformers

Anonymous authors
Paper under double-blind review

Abstract

We address the critical challenge of applying feature attribution methods to the transformer architecture, which dominates current applications in natural language processing and beyond. Traditional attribution methods to explainable AI (XAI) explicitly or implicitly rely on linear or additive surrogate models to quantify the impact of input features on a model's output. In this work, we formally prove an alarming incompatibility: transformers are structurally incapable to align with popular surrogate models for feature attribution, undermining the grounding of these conventional explanation methodologies. To address this discrepancy, we introduce the Softmax-Linked Additive Log-Odds Model (SLALOM), a novel surrogate model specifically designed to align with the transformer framework. SLALOM demonstrates the capacity to deliver a range of insightful explanations with across both synthetic and real-world datasets. We highlight SLALOM's unique efficiency-quality curve by showing that SLALOM can produce explanations with substantially higher fidelity than competing surrogate models or provide explanations of comparable quality at a fraction of their computational costs.

1 Introduction

The transformer architecture (Vaswani et al., 2017) has been established as the status quo in modern natural language processing (Devlin et al., 2018; Radford et al., 2018; 2019; Touvron et al., 2023). However, the current and foreseeable adoption of large language models (LLMs) in critical domains such as the judicial system (Chalkidis et al., 2019) and the medical domain (Jeblick et al., 2023) comes with an increased need for transparency and interpretability. Methods to enhance the interpretability of an artificial intelligence (AI) system are developed in the research area of Explainable AI (XAI, Adadi & Berrada, 2018; Gilpin et al., 2018; Molnar, 2019; Burkart & Huber, 2021). A recent meta-study (Rong et al., 2023) shows that XAI has the potential to increase users' understanding of AI systems and their trust therein. Local feature attribution methods that quantify the contribution of each input to a decision outcome are among the most popular explanation methods, and a variety of approaches have been suggested for the task of computing such attributions (Kasneci & Gottron, 2016; Ribeiro et al., 2016; Sundararajan et al., 2017; Lundberg & Lee, 2017; Covert et al., 2021; Modarressi et al., 2022).

It remains hard to formally define the contribution of an input feature for non-linear functions. Recent work (Han et al., 2022) has shown that many common explanation methods do so by implicitly or explicitly performing a local approximation of the complex black-box function, denoted as f, using a simpler surrogate function g from a predefined class $\mathcal{G}$. For instance, Local Interpretable Model-agnostic Explanations (LIME, Ribeiro et al., 2016) or input gradient explanations (Baehrens et al., 2010) use a linear surrogate model to approximate the black-box f; the model's coefficients can be used as the feature contributions.

Surrogate model explanations have the advantage that they directly describe the behaviour of the model in the proximity of a specific input, i.e., under small perturbations, a property known as *fidelity* (Guidotti et al., 2018; Nauta et al., 2023). Fidelity can be quantified through the difference between the prediction model's outputs and the surrogate model's outputs (Yeh et al., 2019; Zhou et al., 2019). We refer to the notion where the explanations quantitatively describe the prediction model's output under perturbations as *strict fidelity*.

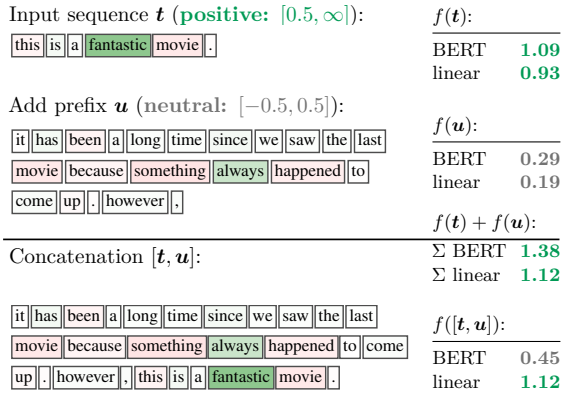

Common Surrogate Models in XAI

Predictive Models	**Surrogate Models**	**Explanation Techniques**
Logistic / Linear Regression, ReLU networks	Linear Model: ✗no non-linearities ✗no interactions	C-LIME, Gradients, IG
GAM, ensembles, boosting	GAM: ✓non-linearities ✗no interactions	Removal-based, e.g. Shapley Values, Local GAM approximation
Transformers	**SLALOM (ours): ✓non-linearities ✓interactions**	**Local SLALOM approximation**

Figure 1: **Transformers cannot be well explained through additive models.** Left: We exemplarily show the log-odds for the outputs of a BERT model and a linear Naïve-Bayes model ("linear") assigning each word a weight trained on the IMDB movie review dataset. We pass two sequences to the models independently and in concatenation. While for the linear model, the output of the concatenated sequence can be described by the sum, this is not the case for BERT. We show that this phenomenon is not due to a non-linearity in this particular model but stems from a general incapacity of transformers to represent additive functions. Right: To overcome this difficulty, we propose SLALOM, a novel surrogate model specifically designed to better approximate transformer models.

An implication of models with high representative capacity and high-fidelity explanations is the *recovery property*: If the true relation f between features and labels in the data is already within the function class $\mathcal{G}$, the model will learn this function and we can effectively reconstruct the original f from the explanations. As an example, suppose that the black-box function we consider is of linear form, i.e., $f(\boldsymbol{x}) = \boldsymbol{w}^\top \boldsymbol{x}$ and has been correctly learned. In this case, a gradient explanation as well as continuous LIME (C-LIME, Agarwal et al., 2021) will recover the original model's parameters up to an offset (Han et al., 2022, Theorem 1). Shapley value explanations (Lundberg & Lee, 2017) possess a comparable relationship: It is known that they correspond to the feature contributions of Generalized Additive Models (GAM, Bordt & von Luxburg, 2023). The significance of recovery properties lies in their role when explanations are leveraged to gain insights into the underlying data. Particularly when XAI is used for scientific applications such as drug discovery (Mak et al., 2023), preserving the path from the input data to the explanation through a learned model is crucial. However, such guarantees can only be provided when surrogate function class $\mathcal{G}$ can effectively mimic the model's learned relation, at least within some local region.

In this study, we demonstrate that the transformer architecture, the main building block of LLMs such as the GPT models (Radford et al., 2019), is inherently incapable of learning additive and linear models on the input tokens, both theoretically and empirically. We formally prove that encoder-only and decoder-only transformers structurally cannot represent additive models due to the attention mechanism's softmax normalization, which necessarily introduces token dependencies over the entire sequence length. An example is illustrated in Figure 1 (left). Our finding that the function spaces represented by additive models and transformers are disjoint when dismissing trivial cases implies that prevalent additive explanations *are insufficient* to model transformers. They cannot possess high fidelity, i.e., they cannot quantitatively describe these models' behavior well. This also undermines the recovery property, therefore highlighting a significant oversight in current XAI practices. As our results suggest that the role of tokens cannot be described through a single score, we introduce the Softmax-Linked Additive Log-Odds Model (SLALOM, cf. Figure 1, right), which represents the role of each input token in two dimensions: The *token value* describes the independent effect of a token, whereas the *token importance* provides a token's interaction weight when combined with other tokens in a sequence. In summary, our work offers the following contributions over the related literature:

(1) We theoretically and empirically demonstrate that common transformer architectures fail to represent GAMs and linear models on the input tokens, jeopardizing current attribution methods' fidelity.

(2) To mitigate these issues, we propose the Softmax-Linked Additive Log-Odds Model (SLALOM), which uses a combination of two scores to quantify the role of input tokens.

(3) We theoretically analyze SLALOM and show that (i) it can be represented by transformers (i.e., the **fidelity property**), (ii) it can be uniquely identified from data (i.e., the **recovery property**), and (iii) it is highly efficient to estimate.

(4) Experiments on synthetic and real-world datasets with common language models (LMs) confirm the mismatch between surrogate models and predictive models, underline that two scores cover different angles of interpretability, and that SLALOM explanations can be computed that have substantially higher fidelity or efficiency than competing techniques.

2 Related Work

Explainability for Transformers. Various methods exist to tackle model explainability (Molnar, 2019; Burkart & Huber, 2021). Furthermore, specific approaches have been devised for the transformer architecture (Vaswani et al., 2017): As the attention mechanism at the heart of transformer models is supposed to focus on relevant tokens, it seems a good target for explainability methods. Several works are turning to attention patterns as model explanation techniques. A central attention-based method is put forward by Abnar & Zuidema (2020), who propose two methods of aggregating raw attentions across layers, *flow* and *rollout*. Brunner et al. (2020) focus on effective attentions, which aim to identify the portion of attention weights actually influencing the model's decision. While these approaches follow a scalar approach considering only attention weights, Kobayashi et al. (2020; 2023) propose a norm-based vector-valued analysis, arguing that relying solely on attention weights is insufficient and the other components of the model need to be considered. Building on the norm-based approach, Modarressi et al. (2022; 2023) further follow down the path of decomposing the transformer architecture, presenting global level explanations with the help of rollout. Beyond that, many more attention-based explanation approaches have been put forward (Chen et al., 2020; Hao et al., 2021; Ferrando & Costa-jussà, 2021; Qiang et al., 2022; Sun et al., 2023; Yang et al., 2023) and relevance-propagation methods such as LRP have been adapted to the transformer architecture (Achtibat et al., 2024). A drawback with these model-specific explanation remains the implementational overhead that is required to adapt these methods for each architecture. On the formal side, there is no explicit method to quantitatively predict the transformer model's behavior under perturbations leaving the fidelity of these explanations unclear. The most intuitive interpretation would be to interpret the attributions as scores of a linear model, i.e., if feature i has a contribution of ϕ_i, removing i should reduce the model output by ϕ_i, giving rise to an implicit linear model. Our work shows that linear models are generally sub-optimal to explain transformers with high fidelity.

Model-agnostic XAI. In contrast to transformer-specific methods, researchers have devised model-agnostic explanations that can be applied without precise knowledge of a model's architecture. Model-agnostic local explanations like LIME (Ribeiro et al., 2016), SHAP (Lundberg & Lee, 2017) and others (Shrikumar et al., 2017; Sundararajan et al., 2017; Smilkov et al., 2017; Xu et al., 2020; Covert et al., 2021, etc.) are a particularly popular class of explanations that are applied to LMs as well (Szczepański et al., 2021; Schirmer et al., 2023; Dolk et al., 2022). Surrogate models are a common subform (Han et al., 2022), which locally approximate a black-box model through a simple, interpretable function.

Linking Models and Explanations. Prior work has distilled the link between classes of surrogate models that can be recovered by explanations (Agarwal et al., 2021; Han et al., 2022, Theorem 3). Notable works in include Garreau & von Luxburg (2020) which provides analytical results on different parametrizations of LIME and Bordt & von Luxburg (2023) which formalizes the connection between Shapley values and GAMs for classical Shapley values as well as n-Shapley values that can also model higher-order interactions.

We contribute to the literature by showing that transformers are inherently incapable to represent GAMs or linear models, casting doubts on the fidelity of LIME, SHAP, and attention-based attribution methods that can be understood as an implicit linear models when applied to transformers. We show that additive scores are insufficient to predict behavior of transformers, leaving us with no method that enables strict fidelity. To bridge this gap we provide SLALOM, a novel surrogate model with substantially increased fidelity and a recovery property for transformers.

3 Preliminaries

3.1 Input and output representations

In this work, we focus on classification problems of token sequences. For the sake of simplicity, we initially consider a 2-class classification problem with labels $y \in \mathcal{Y} = \{0, 1\}$. We will outline how to generalize our approach to multi-class problems in Appendix C.1.

The input consists of a sequence of tokens $\boldsymbol{t} = [t_1, \ldots, t_{|\boldsymbol{t}|}]$ where $|\boldsymbol{t}| \in 1, \ldots, C$ is the sequence length that can span at most C tokens (the context length). The tokens stem from a finite size vocabulary $\mathcal{V}$, i.e., $t_i \in \mathcal{V}, i = 1, \ldots, |\boldsymbol{t}|$. To transform the tokens into a representation amenable to processing with computational methods, the tokens need to be encoded as numerical vectors. To this end, an embedding function $\boldsymbol{e} : \mathcal{V} \to \mathbb{R}^d$ is used, where d is the embedding dimension. Let $\boldsymbol{e}_i = \boldsymbol{e}(t_i)$ be the embedding of the i-th token such that the entire sentence is embedded in a matrix $\boldsymbol{E} = [\boldsymbol{e}_1, \ldots, \boldsymbol{e}_{|\boldsymbol{t}|}]^\top \in \mathbb{R}^{|\boldsymbol{t}| \times d}$. The output is given by a logit vector $\boldsymbol{l} \in \mathbb{R}^{|\mathcal{Y}|}$, such that softmax$(\boldsymbol{l})$ contains individual class probabilities.

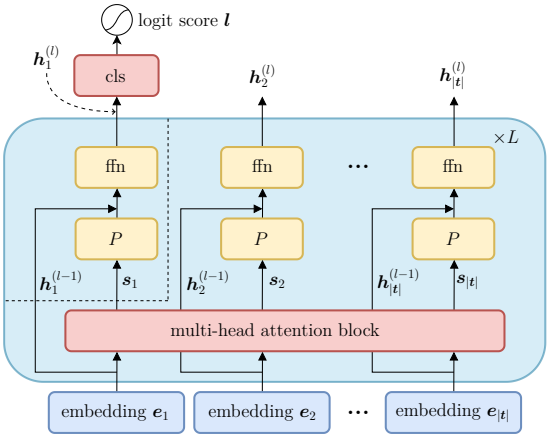

Figure 2: **Transformer architecture.** In each layer, input embeddings $\boldsymbol{h}_i^{(l-1)}$ for each token i are transformed into output embeddings $\boldsymbol{h}_i^{(l)}$. When detaching the part prior to the classification head ("cls"), we see that the output only depends on the last embedding $\boldsymbol{h}_1^{(L-1)}$ and attention output $\boldsymbol{s}_1$.

3.2 The common transformer architecture

Many popular LMs follow the transformer architecture introduced by Vaswani et al. (2017) with only minor modifications. We will introduce the most relevant building blocks of the architecture in this section. A complete formalization is given in Appendix B.1. A schematic overview of the architecture is visualized in Figure 2. Let us denote the input embedding of token $i = 1, \ldots, |\boldsymbol{t}|$ in layer $l \in 1, \ldots, L$ by $\boldsymbol{h}_i^{(l-1)} \in \mathbb{R}^d$, where $\boldsymbol{h}_i^{(0)} = \boldsymbol{e}_i$. The core component of the attention architecture is the attention head.[1] For each token, a *query*, *key*, and a *value* vector are computed by applying an affine-linear transform to the input embeddings. Keys and queries are projected onto each other and normalized by a row-wise softmax operation resulting in attention weights $\alpha_{ij} \in [0, 1]$, denoting how much token i is influenced by token j. The attention output for token i can be computed as $\boldsymbol{s}_i = \sum_{j=1}^{|\boldsymbol{t}|} a_{ij} \boldsymbol{v}_j$, where $\boldsymbol{v}_j \in \mathbb{R}^{d_h}$ denotes the value vector for token j. The final $\boldsymbol{s}_i$ are projected back to dimension d by a projection operator $P : \mathbb{R}^{d_h} \to \mathbb{R}^d$ before they are added to the corresponding input embedding $\boldsymbol{h}_i^{(l-1)}$ as mandated by skip-connections. The sum is then transformed by a nonlinear function that we denote by ffn : $\mathbb{R}^d \to \mathbb{R}^d$, finally resulting in a transformed embedding $\boldsymbol{h}_i^{(l)}$. This procedure is repeated iteratively for layers $1, \ldots, L$ such that we finally arrive at output embeddings $\boldsymbol{h}_i^{(L)}$. To perform classification, a classification head cls : $\mathbb{R}^d \to \mathbb{R}^{|\mathcal{Y}|}$ is put on top of a token at some index r (how this token is chosen depends on the architecture, common choices include $r \in \{1, |\boldsymbol{t}|\}$), such that we get the final logit output $\boldsymbol{l} = \text{cls}\left(\boldsymbol{h}_r^{(L)}\right)$. The logit output is transformed to a probability vector via another softmax operation. Note that in the two-class case, we obtain the log-odds $F(\boldsymbol{t})$ by taking the difference (Δ) between the two logits, i.e., $F(\boldsymbol{t}) \coloneqq \log \frac{p(y=1|\boldsymbol{t})}{p(y=0|\boldsymbol{t})} = \Delta(\boldsymbol{l}) = \boldsymbol{l}_1 - \boldsymbol{l}_0$.

3.3 Encoder-Only and Decoder-Only models

Practical implementations introduce subtle modifications into the process described previously(see Appx. C.2 for details). The most relevant distinction is made between *encoder-only* models, that include BERT (Devlin et al., 2018) and its variants, and *decoder-only* models such as the GPT models (Radford et al., 2018; 2019).

[1] Although we only formalize a single head here, our theoretical results cover multiple heads as well

Encoder-only models. Considering BERT as an example of an encoder-only model, the first token is used for the classification, i.e, $r = 1$. Usually, a special token `[CLS]` is prepended to the text at position 1, however this is not strictly necessary for the functioning of the model.

Decoder-only models. In contrast, decoder-models like GPT-2 (Radford et al., 2019) add the classification head on top of the last token for classification, i.e., $r = |\boldsymbol{t}|$. A key difference is that in GPT-2 and other decoder-only models, a causal mask is laid over the attention matrix, resulting in $\alpha_{i,j} = 0$ for $j > i$. This encodes the constraint that tokens can only attend to themselves or to previous ones.

4 Analysis

Let us initially consider a transformer with only a single layer and head. Our first insight is that the classification output can be determined only by two values: the input embedding at the classification token r, $\boldsymbol{h}_r^{(0)}$, and the attention output s_r. This can be seen when plugging in the different steps:

$$F(\boldsymbol{t}) = \Delta\left(\mathrm{cls}(\boldsymbol{h}_r^{(1)})\right) = \Delta\left(\mathrm{cls}\left(\mathrm{ffn}(\boldsymbol{h}_r^{(0)} + \boldsymbol{P}(\boldsymbol{s}_r))\right)\right) := g(\boldsymbol{h}_r^{(0)}, \boldsymbol{s}_r) = g\Big(\boldsymbol{h}_r^{(0)}, \sum_{j=1}^{|\boldsymbol{t}|} a_{rj}\boldsymbol{v}_j\Big). \tag{1}$$

The attention output is given by a sum of the token value vectors $\boldsymbol{v}_j$ weighted by the respective attention weights α_{rj}.

4.1 Transformers cannot represent additive models

We now consider how this architecture would represent a linear model. In this model, each token is assigned a weight $w : \mathcal{V} \to \mathbb{R}$. The output obtained by adding weights and an offset $b \in \mathbb{R}$:

$$F([t_1, t_2, \ldots, t_{|\boldsymbol{t}|}]) \stackrel{!}{=} b + \sum_{i=1}^{|\boldsymbol{t}|} w(t_i). \tag{2}$$

The transformer gives rise to an interesting observation when considering token sequences of identical tokens but of different lengths, i.e., $[\tau], [\tau, \tau]$, etc. We first note that the sum of the attention scores is bound to be $\sum_{j=1}^{|\boldsymbol{t}|} a_{rj} = 1$. The output of the attention head will thus be a weighted average of the value vectors $\boldsymbol{v}_i$. As the value vectors $\boldsymbol{v}_j(t_j)$ are determined purely by the input tokens t_j, for a sequence of identical tokens, we will have the same value vectors, resulting in identical vectors being averaged. In summary, this renders the transformer incapable to differentiate between sequences of different lengths. We are now ready to state our result, which formalizes this intuition.

Proposition 4.1 (Single-layer transformers cannot represent generalized additive models (GAMs))**.** *Let $\mathcal{V}$ be a vocabulary and $C \geq 2, C \in \mathbb{N}$ be a maximum sequence length (context length). Let $w_i : \mathcal{V} \to \mathbb{R}, \forall i \in 1, ..., C$ be any mapping that assigns a token encountered at position i a numerical score including at least one token $\tau \in \mathcal{V}$ with non-zero weight $w_i(\tau) \neq 0$ for some $i \in 2, \ldots, C$. Let $b \in \mathbb{R}$ be an arbitrary offset. Then, there exists no parametrization of the encoder or decoder single-layer transformer F such that for every sequence $\boldsymbol{t} = [t_1, t_2, \ldots, t_{|\boldsymbol{t}|}]$ with length $|\boldsymbol{t}| \leq C$, the output of the transformer network is equivalent to $F([t_1, t_2, \ldots, t_{|\boldsymbol{t}|}]) = b + \sum_{i=1}^{|\boldsymbol{t}|} w_i(t_i)$.*

Proof Sketch. We prove the statement by concatenating the token τ to sequences of different length. We then show that the inputs to the final part g of the transformer will be independent of the sequence length. Due to g being deterministic, the output will also be independent of the sequence length. This is contradictory to the GAM model with a weight $w_j(\tau) \neq 0$ requiring different outputs for sequences of length $j-1$ and j. Formal proofs for all results can be found in Appendix B. □

In simple terms, the proposition states that the transformer cannot represent any GAMs on sequences of more than one token besides constant functions or those fully determined by the first input token. Importantly, the class of functions stated in the above theorem includes the prominent case of linear models in Eqn. (1), where each token has a certain weight w independent of its position in the input vector (i.e., $w_i \equiv w, \forall i$, see Corollary B.2). We would like to emphasize that this statement includes the converse:

Corollary 4.2. *Transformers whose outputs are not constant or fully determined by the first token of the input sequence cannot be functionally equivalent to an additive model.*

4.2 Transformer networks with multiple layers cannot represent additive models

In this section, we will show how the argument can be extended to multi-layer transformer networks. Denote by $\boldsymbol{h}_i^{(l-1)}$ the input embedding of the ith token at the lth layer. The output is governed by the recursive relation

$$\boldsymbol{h}_i^{(l)} = \mathrm{ffn}_l(\boldsymbol{h}_i^{(l-1)} + \boldsymbol{P}_l(\boldsymbol{s}_i)) = g_l(\boldsymbol{h}_i^{(l-1)}, \boldsymbol{s}_i). \tag{3}$$

Exploiting the similar form allows us to generalize the main results to more layers recursively.

Corollary 4.3 (Multi-Layer transformers cannot learn linear models either)**.** *Under the same conditions as in Proposition 4.1, a stack of multiple transformer blocks as in the model F neither has a parametrization sufficient to represent the linear model.*

Practical considerations. The transformer model in our analysis contains one slight deviation from the transformer architecture deployed in practice as it does not consider positional embeddings that are added on the token embeddings. However, this does not have major ramifications in practice: While the transformer would be able to differentiate between sequences of different lengths with positional embeddings in theory, the softmax operation must be inverted for any input sequence by the linear feed-forward block that follows the attention mechanism. This is a highly nonlinear operation and the number of possible sequences grows exponentially with the context length and vocabulary size. Learning-theoretic considerations suggest that this inversion is impossible for reasonably-sized networks as outlined in Appendix C.2. We will confirm our results with empirical findings obtained exclusively on non-modified models with positional embeddings.

5 A Surrogate Model for Transformers

In the previous section, we theoretically established that transformer models struggle to represent additive functions. While this must not necessarily be considered a weakness, it certainly casts doubts on the suitability of additive models as surrogate models for explanations of transformers. For a principled approach, we consider the following four requirements to be of importance:

(1) **Interpretability.** The surrogate model's parameters should be inherently interpretable.

(2) **Learnability.** The surrogate model should be easiliy representable by common transformers.

(3) **Recovery.** If the predictive model falls into the surrogate model's class, the fitted surrogate model's parameters should match those of the predictive model.

(4) **Efficiency.** The surrogate model should be efficient to estimate even for larger models.

5.1 The Softmax-Linked Additive Log-Odds Model

To meet the requirements, we propose a novel discriminative surrogate model that explicitly models the behavior of the softmax function. Instead of only assigning a single weight w to each token, we separate two characteristics: We introduce the *token importance* as a mapping $s : \mathcal{V} \to \mathbb{R}$ and a *token value* in form of a mapping $v : \mathcal{V} \to \mathbb{R}$. Subsequently, we consider the following discriminative model:

$$F(\boldsymbol{t}) = \log \frac{p(y=1|\boldsymbol{t})}{p(y=0|\boldsymbol{t})} = \sum_{\tau_i \in \boldsymbol{t}} \alpha_i(\boldsymbol{t}) v(t_i), \quad \text{where } \alpha_i(\boldsymbol{t}) = \frac{\exp(s(t_i))}{\sum_{t_j \in \boldsymbol{t}} \exp(s(t_j))}. \tag{4}$$

Due to the shift invariance of the softmax function, we observe that the mappings s and s' given by $s'(\tau) = s(\tau) + \delta$ result in the same softmax-score and thus the same log-odds model for any input $\boldsymbol{t}$. Therefore, the parameterization would not be unique. To this end, we introduce a *normalization constraint* on the sum of token importances for uniqueness. Formally, we constrain it to a user-defined constant $\gamma \in \mathbb{R}$ such

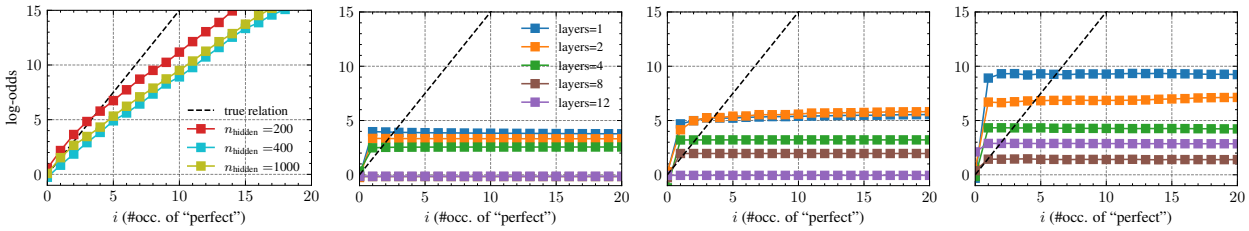

(a) Linear Model (b) BERT (c) DistilBERT (d) GPT-2

Figure 3: **Transformers fail to learn linear models.** We train different models on a synthetically sampled dataset where the log-odds obey a linear relation to the features. Fully connected models (2-layer ReLU networks with different hidden layer widths) capture the linear form of the relationship well despite some estimation error (a). However, common transformer models fail to model this relationship and output almost constant values (b)-(d). This does not change with more layers.

that $\sum_{\tau \in \mathcal{V}} s(\tau) = \gamma$, where natural choices include $\gamma \in \{0, 1\}$. We refer to the discriminative model given in Eqn. (4) together with the normalization constraint as the *softmax-linked additive log-odds model* (SLALOM).

As common in surrogate model explanations, we can fit SLALOM to a predictive model's outputs globally or locally and use tuples of token importance scores and token values scores, $(v(\tau), s(\tau))$ to give explanations for an input token τ. While the value score provides an absolute contribution of τ to the output, its token importance $s(\tau)$ determines its weight with respect to the other tokens. For instance, if only one token τ is present in a sequence, the output is only determined by its value score $v(\tau)$. However, in a sequence of multiple tokens, the importance of each token with respect to the others – and thereby the contribution of this token's value – is determined by the token importance scores s. This intuitive relation makes SLALOM interpretable, thereby satisfying Property (1).

5.2 Theoretical properties of SLALOM

We analyze the proposed SLALOM theoretically to ensure that it fulfills Properties (2) and (3), Learnability and Recovery, and subsequently provide efficient algorithms to estimate its parameters (4). First, we show that – unlike linear models, SLALOMs can be easily learned by transformers.

Proposition 5.1 (Transformers can fit SLALOM)**.** *For any mapping s, v and a transformer with an embedding size d and head dimension d_h with $d, d_h \geq 3$, there exists a parameterization of the transformer to reflect SLALOM in Equation* (4) *together with the normalization constraint.*

This statement can be proven by explicity constructing the corresponding weight matrix. This proposition highlights that – unlike linear models – there are simple ways for the transformer to represent relations governed by SLALOMs. We demonstrate this empirically in our experimental section and conclude that SLALOM fulfills Property (2). For Property (3), Recovery, we make the following proposition:

Proposition 5.2 (Recovery of SLALOMs)**.** *Suppose query access to a model G that takes sequences of tokens $\boldsymbol{t}$ with lengths $|\boldsymbol{t}| \in 1, \ldots, C$ and returns the log-odds according to a non-constant SLALOM on a vocabulary $\mathcal{V}$, normalization constant $\tau \in \mathbb{R}$, but with unknown parameter mappings $s : \mathcal{V} \to \mathbb{R}$, $v : \mathcal{V} \to \mathbb{R}$. For $C \geq 2$, we can recover the true mappings s, v with $2|\mathcal{V}| - 1$ forward passes of F.*

This statement confirms property (3) and shows that SLALOM can be uniquely reidentified when we rule out the corner case of constant models.

Complexity considerations. Computational complexity can be a concern for XAI methods. To estimate exact Shapley values, the model's output on exponentially many feature coalitions needs to be evaluated. However, as the proof of Proposition 5.2 shows, to estimate SLALOM's parameters for an input sequence of $\mathcal{V}$ tokens, only $2|\mathcal{V}| - 1$ forward passes are required, verifying Property (4). We empirically show that computing SLALOM explanations is about **5× faster** than computing SHAP explanations when using the same number of samples in our experimental section.

5.3 Numerical Algorithms for computing SLALOMs

Having derived SLALOM as a better surrogate model, we make two key implementation choices for a practical used as an explanation technique. First, we can control the sample set of features and labels by the predictive model that is used to fit SLALOM. Second, we can use different optimization strategies. We suggest two algorithms to fit SLALOMs post-hoc on input-output pairs of a trained predictive model:

SLALOM-`eff`. The first version of the algorithm to fit SLALOM models is designed for maximum efficiency while maintaining reasonable performance across several XAI metrics. Obtaining a large dataset of input-output pairs can incur substantial computational costs as a forward pass of the models needs to be executed for each sample. To speed up this process, SLALOM-`Eff` uses very short sequences (we use only two tokens in this work) randomly sampled from the vocabulary for this purpose. To efficiently fit the surrogate model, we perform stochastic gradient descent on SLALOM's parameters using the mean-squared-error loss. SLALOM-`eff` is our default technique used unless stated otherwise.

SLALOM-`fidel`. We provide another technique to fit SLALOM optimized for maximum fidelity under input perturbations such as token removals. To explain a specific sample, we sample input where we remove up to K randomly sampled tokens. The sequences with tokens removed and their models scores are used to fit the model, similar as done in LIME (Ribeiro et al., 2016). Instead of SGD, we can leverage optimizers for Least-Square-Problems to fit the parameters iteratively, however incurring a higher latency. We provide details and pseudocode for both fitting routines in Appendix D.

5.4 Relating SLALOM scores to linear attributions

Importantly, SLALOM scores can be readily converted to locally linear interpretability scores where necessary. For this purpose, a differentiable model for soft removals is required. We consider the weighted model:

$$F(\boldsymbol{\lambda}) = \frac{\sum_{t_i \in \boldsymbol{t}} \lambda_i \exp(s(t_i)) v(t_i)}{\sum_{t_i \in \boldsymbol{t}} \lambda_i \exp(s(t_i))}, \tag{5}$$

where $\lambda_i = 1$ if a token is present and $\lambda_i = 0$ if it is absent. We observe that setting $\lambda_i = 0$ has the desired effect of making the output of the soft-removal model equivalent to that of the standard SLALOM on a sequence without this token. Taking the gradients at $\boldsymbol{\lambda} = \mathbf{1}$ we obtain $\frac{\partial F}{\partial \lambda_i}\Big|_{\boldsymbol{\lambda}=\mathbf{1}} \propto v(t_i)\exp(s(t_i))$, which can be used to rank tokens according the linearized attributions. We defer the derivation to Appendix B.7 and refer to these scores as *linearized* SLALOM scores.

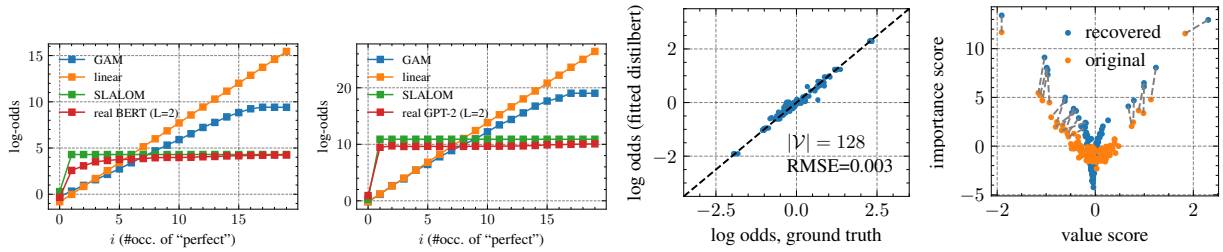

(a) BERT (b) GPT-2 (c) Recovering Log-Odds (d) Recovering Params.

Figure 4: **SLALOM describes outputs of transformer models well (a, b).** Fitting SLALOM to the outputs of the real models. Despite having $C/2$=15× more parameters than the SLALOM model, the linear and GAM models does not match the transformer behavior. We provide another empirical counterexample and additional quantitative results in Appendix F.1. **Recovering SLALOMs.** We observe that we can recover the original logit-scores by fitting SLALOM on a 2-layer DistilBERT model (c) and we see a strong connection between original SLALOM parameters and the recovered ones (d). More results in Appendix F.2.

6 Experimental Evaluation

We run a series of experiments to show the mismatch between surrogate model explanations and the transformers. Specifically, we verify that (1) real transformers fail to learn additive models, (2) SLALOM better captures transformer output, (3) SLALOM models can be reidentified from fitted models with tolerable error, (4) SLALOM scores are versatile and align well with linear attribution scores and human attention, and (5) that SLALOM performs well in faithfulness metrics and has substantially higher fidelity than competing techniques. For experiments (1)-(3), we require knowledge of the ground truth, and therefore use synthetic datasets. To demonstrate the practical strengths of our method, all the experiments for (4) and (5) are conducted on real-world datasets, and in comparison with state-of-the-art XAI techniques.

6.1 Experimental Setup

LM architectures. We study three representative transformer language model architectures in our experiments. In sequence classification, mid-sized transformer LMs are most popular on platforms such as the Huggingface hub (Huggingface, 2023) often based on the BERT-architecture (Devlin et al., 2018), which is reflected in our experimental setup. To represent the family of encoder-only models, we deploy BERT (Devlin et al., 2018) and DistilBERT (Sanh et al., 2019). We further experiment with GPT-2 (Radford et al., 2019), which is a decoder-only model. We use the `transformers` framework to run our experiments. While not the main scope of this work, we show that due to its model-agnostic nature, SLALOM can be applied to LLMs with up to 7B parameters and non-transformer models such as Mamba (Gu & Dao, 2023) or BLOOM (Le Scao et al., 2023) with plausible results due to its general expressivity in Appendix F.7.

Datasets. We use two real-world datasets for sentiment classification. Specifically, we study the IMDB dataset, consisting of movie reviews (Maas et al., 2011) and Yelp-HAT, a dataset of Yelp reviews, for which human annotators have provided annotations on which tokens are relevant for the classification outcome (Sen et al., 2020). We provide additional details on hyperparameters, training and datasets in Appendix E.

6.2 Evaluation with Known Ground Truth

Transformers fail to capture linear relationships. We empirically verify the claims made in Proposition 4.1 and Corollary 4.3. To ascertain that the underlying relation captured by the models is additive, we resort to a synthetic dataset. The dataset is created as follows: First, we sample different sequence lengths from a binomial distribution with a mean of 15. Second, we sample words independently from a vocabulary of size 10. This vocabulary was chosen to include positive words, negative words, and neutral words, with manually assigned weights $w \in \{-1.5, -1, 0, 1, 1.5\}$, that can be used to compute a linear log-odds model. We evaluate this model and finally sample the sequence label accordingly, thereby ensuring a linear relation between input sequences and log-odds. We train transformer models on this dataset and evaluate them on sequences containing the same word ("perfect") multiple times. Our results in Figure 3 show that the models fail to capture the relationship regardless of the model or number of layers used. In Appendix A, we show how this undermines the recovery property with Shapley value explanations.

Fitting SLALOM as a surrogate to transformer models. Having demonstrated the mismatch between additive functions and transformers, we turn to SLALOM as a more suitable surrogate model. As shown in Proposition 5.1, transformers can easily fit SLALOMs, which is why we hypothesize that they should model the output of such a model well in practice. We fit the different surrogate models on a dataset of input sequences and real transformer outputs from our synthetic dataset and observe that linear models and GAMs fail to capture the relationship learned by the transformer as shown in Figure 4(a, b). On the contrary, SALO manages to model the relationship well, even if it has considerably less trainable parameters than the GAM.

Verifying recovery. We run an experiment to study whether, unlike linear models, SLALOM can be fitted and recovered by transformers. To test this, we sample a dataset that exactly follows the distribution given by SLALOM. We then train transformer models on this dataset. The results in Figure 4(c, d) show that the surrogate model fitted on transformer outputs as a post-hoc explanation recovers the correct log-odds mandated by SLALOM (c) and that there is a good correspondence between the true model's parameters and the recovered model's parameters (d).

LM	values v	importances s	lin.
BERT	0.619 ± 0.01	0.349 ± 0.01	**0.626** ± 0.01
Distil-BERT	0.692 ± 0.01	0.373 ± 0.01	**0.693** ± 0.01
GPT-2	0.618 ± 0.01	0.292 ± 0.01	**0.619** ± 0.01
average	0.643	0.338	**0.646**

(a) Measuring average rank-correlation (Spearman) between Naive-Bayes scores and SLALOM scores. Linearized performs best.

LM	values v	importances s	lin.
Bert	0.786 ± 0.01	**0.807** ± 0.01	0.801 ± 0.01
Distil-BERT	**0.688** ± 0.01	0.681 ± 0.01	0.686 ± 0.01
GPT-2	0.674 ± 0.01	**0.685** ± 0.01	0.683 ± 0.01
average	0.716	**0.724**	0.724

(b) Measuring average AU-ROC between SLALOM explanations and human token attention. The importance scores are clearly and most strongly predictive of human attention.

	SLALOM-`fidel`		SLALOM-`eff`						
LM	v-scores	lin.	v-scores	lin.	LIME	SHAP	IG	Grad	LRP
BERT	0.025 ± 0.002	**0.023** ± 0.001	0.031 ± 0.002	0.031 ± 0.002	0.024 ± 0.002	0.026 ± 0.003	0.557 ± 0.034	0.611 ± 0.033	0.030 ± 0.006
DistilBERT	0.028 ± 0.003	0.024 ± 0.002	0.027 ± 0.002	0.027 ± 0.002	0.027 ± 0.003	0.029 ± 0.003	0.495 ± 0.027	0.508 ± 0.028	**0.023** ± 0.002
GPT-2	0.052 ± 0.008	0.050 ± 0.008	0.089 ± 0.008	0.089 ± 0.008	0.230 ± 0.017	**0.042** ± 0.005	0.454 ± 0.022	0.493 ± 0.023	0.069 ± 0.010
average	0.035 ± 0.004	**0.032** ± 0.004	0.049 ± 0.004	0.049 ± 0.004	0.094 ± 0.007	**0.032** ± 0.003	0.502 ± 0.028	0.537 ± 0.028	0.041 ± 0.006

(c) Area Over Perturbation Curve for deletion. Linearized scores and SHAP performs best in the XAI metric.

Table 1: Evaluation of SLALOM scores ("values", "importance", "lin.") with std. errors across explanation quality measures highlights that SLALOM's different scores serve different purposes. IMDB dataset shown.

6.3 Examining Real-World Predictions from Different Angles

We increase difficulty and deploy SLALOM (fitted using SLALOM-`eff`) to explain predictions on real-world datasets. As there is no ground truth for these datasets, it is challenging to evaluate the quality of the explanations (Rong et al., 2022). To better understand SLALOM explanations, we study them from several angles: We compare to linear scores obtained when fitting a Naïve-Bayes Bag-of-Words (BoW) model, scores on removal and insertion benchmarks (Tomsett et al., 2020; DeYoung et al., 2020), the human attention scores available on the Yelp-HAT dataset (Sen et al., 2020), and provide qualitative results.

Explaining Sentiment Classification. We show qualitative results for explaining a movie review in Figure 5. The figure shows that both negative and positive words are assigned high importance scores but have value scores of different signs. Furthermore, we see that some words ("the") have positive value scores, but a very low importance. This means that they lead to positive scores on their own but are easily overruled by other words. We compare the SLALOM scores obtained on 100 random test samples to a linear Naïve-Bayes model (obtained though counting class-wise word frequencies) as a surrogate ground truth in Table 1a through the Spearman rank correlation. We observe good agreement with the value scores v and the combined linearized SLALOM scores ("lin", see Section 5.4).

Predicting Human Attention. To study alignment with a user perspective, we predict human attention from SLALOM scores. We compute AU-ROC for predicting annotated human attention as suggested in Sen et al. (2020) in Table 1b. We use absolute values of all signed explanations as human attention is unsigned as well. In contrast to the previous experiments, where value scores were more effective than importances, we observe that the importance scores are best at predicting where the human attention is placed. In summary, these findings highlight that the two scores serve different purposes and cover different dimensions

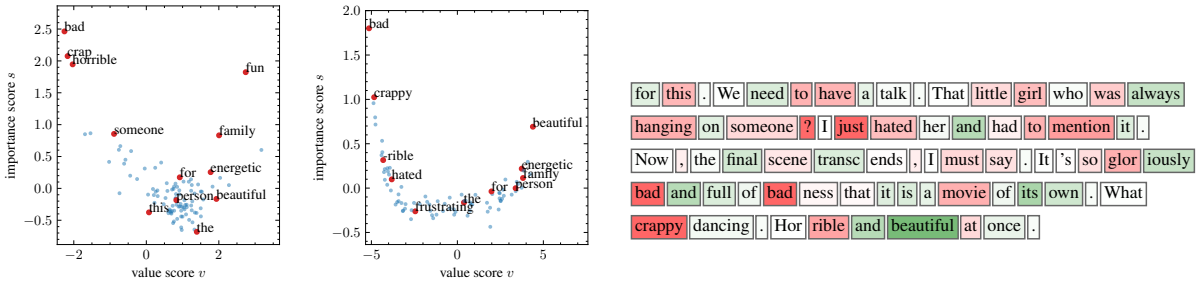

(a) BERT (b) GPT-2 (c) Token highlighting (linearized SLALOM, GPT-2)

Figure 5: Explaining a real review with SLALOM (qualitative results). SLALOM assigned two scores to each token and can be used to compute attributions. See Figure 12 (Appendix) for fully annotated plots.

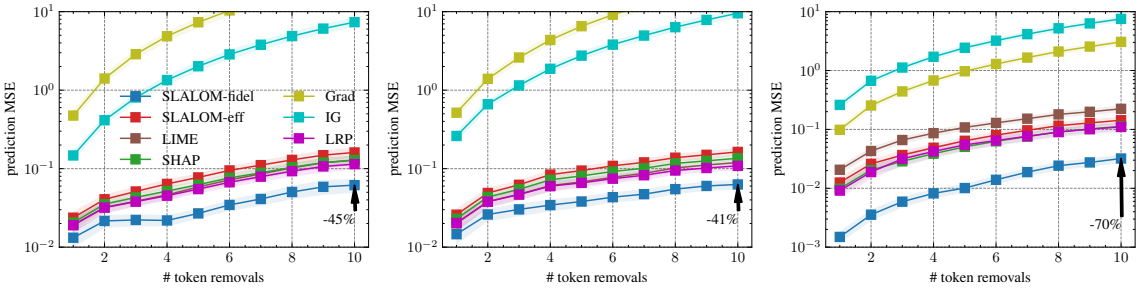

(a) BERT (b) DistilBERT (c) GPT-2

Figure 6: **Assessing Strict Fidelity.** We plot the MSE for predicting model outputs under token removal and find that SLALOMs predictions have up to 70% less error than the closest competitor when up to 10 random tokens from a sentence are removed (log-y plots). We interpret LRP scores as a linear model.

of interpretability. SLALOM offers higher flexibility through its 2-dimensional representation. We show that SLALOM's results for BoW correlations and human attention prediction are in the same range and often outperform competing techniques in Appendix F.3.2, but defer a comparative analysis to the next sections.

Assessing Strict Fidelity. Having established the roles of its components, we verify that SLALOM can produce explanations that have substantially higher fidelity than competing surrogate or non-surrogate explanation techniques. To assess this, we remove up to 10 tokens from the input sequences and use the explanations to predict the change in model output using the surrogate model (SLALOM or linear). We compare the two SLALOM versions to baselines such as LIME (Ribeiro et al., 2016), Kernel-SHAP (Lundberg & Lee, 2017), Gradients (Simonyan et al., 2013), and Integrated Gradients (IG, Sundararajan et al., 2017) and layer-wise relevance propagation (LRP) for transformers (Achtibat et al., 2024), a non-surrogate technique. We report the Mean-Squared-Error (MSE) between the predicted change and the observed change when running the model on the modified inputs in Figure 6. We observe that SLALOM-`fidel` offers substantially higher fidelity with a reduction of 70% in MSE for predicting the output changes over the second-best method (LRP). Other surrogate approaches and LRP remain cluttered together, potentially highlighting the frontier of maximum fidelity possible with a linear surrogate model.

Evaluating XAI Metrics. There are several other metrics to quantify quality of explanations and to compare different explanation techniques. As a sanity check and to show that SLALOM explanations do not lag behind other techniques in established metrics, we run the classical insertion/removal benchmarks (Tomsett et al., 2020). For the insertion benchmark, we successively add the tokens with the highest attributions to the sample which should result in a high score for the target class. We iteratively insert more tokens and compute the "Area Over the Perturbation Curve" (AOPC, see DeYoung et al. (2020)), which should be low for insertion. This metric quantifies the alignment of explanations and model behavior but only considers the feature ranking and not the assigned score. For surrogate techniques (LIME, SHAP, SLALOM) we use 5000 samples each. Our results in Tab. 1c highlight that linearized SLALOM scores outperform LIME and LRP and perform on par with SHAP. Removal results for IMDB and results on YELP with similar findings are deferred to Table 11 (Appendix). In conclusion, this shows that on top of SLALOM's desirable properties, it does not lag behind other techniques in common evaluation metrics.

Approach	Avg. Time (s)
Grad	0.01 ± 0.00
IG	0.02 ± 0.00
LRP	0.02 ± 0.00
SLALOM-`eff`	2.03 ± 0.01
SLALOM-`fidel`	3.77 ± 0.24
LIME	3.93 ± 0.19
SHAP	11.56 ± 0.03

Table 2: Runtime comparison using 5000 samples to estimate surrogate models.

Computational Costs. Finally, we take a look at the computational costs of the methods, which are mainly determined by sampling the dataset to fit the surrogate model. We provide the runtimes to explain a sample on our hardware when using 5000 samples to estimate surrogates in Table 2 with more results in Appendix F.6. We observe that SHAP incurs the highest computational burden. Among surrogate model explanations SLALOM-`eff` is the most efficient, being about 5× more efficient that SHAP and 2× more

efficient than LIME. Nevertheless, non-surrogate techniques are far more efficient as they require only one or few (IG steps) forward or backward passes, but suffer from other disadvantages (e.g., implementation effort, no explicit way to predict model behavior). Overall, our results highlight that the two SLALOM fitting routines can produce explanations of comparable utility as other surrogate models at a fraction of the costs, or produce explanations with higher fidelity at similar costs due to structurally better alignment between surrogate and predictive models.

7 Discussion and Conclusion

In this work, we established that transformer networks are inherently incapable of representing linear or additive models commonly used for feature attribution. We prove that the function spaces learnable by transformers and linear models are disjoint when ruling out trivial cases. This may explain similar incapacities observed in time-series forecasting (Zeng et al., 2023), where they seem incapable of representing certain relations. To address this shortcoming, we have introduced the Softmax-Linked Additive Log-Odds Model (SLALOM), a surrogate model for explaining the influence of features on transformers and other complex LMs through a two-dimensional representation.

Our work still has certain limitations that could potentially be addressed in future work. SLALOM is specifically designed to explain the behavior of transformer models and therefore aligned with the classes of functions commonly represented by transformers. However, it would not be a suitable choice to explain models capturing a linear relationship. We therefore recommend using SLALOM only when the model is known to have attention-like non-linearities. To complement this theoretical foundation, future work will include further evaluation of SLALOM from a user-centric perspective, for instance, on human-centered evaluation frameworks (Colin et al., 2022). From a broader perspective, we hope that this research paves the way for advancing the interpretability and theoretical understanding of widely adopted transformer models.

Broader Impact Statement

This paper presents theoretical work on better understanding feature attributions in the transformer framework. We advise using caution when using our XAI technique or other model explanation as all explanations present only a simplified view of the complex ML model. Besides that, we do not see any immediate impact which we feel must be specifically highlighted here.

References

Samira Abnar and Willem Zuidema. Quantifying attention flow in transformers. In *Proceedings of the 58th Annual Meeting of the Association for Computational Linguistics*, pp. 4190–4197, 2020.

Reduan Achtibat, Sayed Mohammad Vakilzadeh Hatefi, Maximilian Dreyer, Aakriti Jain, Thomas Wiegand, Sebastian Lapuschkin, and Wojciech Samek. Attnlrp: Attention-aware layer-wise relevance propagation for transformers. In *Forty-first International Conference on Machine Learning*, 2024.

Amina Adadi and Mohammed Berrada. Peeking inside the black-box: a survey on explainable artificial intelligence (xai). *IEEE access*, 2018.

Sushant Agarwal, Shahin Jabbari, Chirag Agarwal, Sohini Upadhyay, Steven Wu, and Himabindu Lakkaraju. Towards the unification and robustness of perturbation and gradient based explanations. In *International Conference on Machine Learning*, pp. 110–119. PMLR, 2021.

Nabiha Asghar. Yelp dataset challenge: Review rating prediction. *arXiv preprint arXiv:1605.05362*, 2016.

David Baehrens, Timon Schroeter, Stefan Harmeling, Motoaki Kawanabe, Katja Hansen, and Klaus-Robert Müller. How to explain individual classification decisions. *The Journal of Machine Learning Research*, 11: 1803–1831, 2010.

Peter Bartlett, Vitaly Maiorov, and Ron Meir. Almost linear vc dimension bounds for piecewise polynomial networks. *Advances in neural information processing systems*, 11, 1998.

Sebastian Bordt and Ulrike von Luxburg. From shapley values to generalized additive models and back. In *International Conference on Artificial Intelligence and Statistics*, pp. 709–745. PMLR, 2023.

Gino Brunner, Yang Liu, Damian Pascual, Oliver Richter, Massimiliano Ciaramita, and Roger Wattenhofer. On identifiability in transformers. 2020.

Nadia Burkart and Marco F Huber. A survey on the explainability of supervised machine learning. *Journal of Artificial Intelligence Research*, 70:245–317, 2021.

Javier Castro, Daniel Gómez, and Juan Tejada. Polynomial calculation of the shapley value based on sampling. *Computers & Operations Research*, 36(5):1726–1730, 2009.

Ilias Chalkidis, Ion Androutsopoulos, and Nikolaos Aletras. Neural legal judgment prediction in english. In *Proceedings of the 57th Annual Meeting of the Association for Computational Linguistics*, pp. 4317–4323, 2019.

Hanjie Chen, Guangtao Zheng, and Yangfeng Ji. Generating hierarchical explanations on text classification via feature interaction detection. *arXiv preprint arXiv:2004.02015*, 2020.

Julien Colin, Thomas Fel, Rémi Cadène, and Thomas Serre. What i cannot predict, i do not understand: A human-centered evaluation framework for explainability methods. *Advances in neural information processing systems*, 35:2832–2845, 2022.

Ian Covert, Scott Lundberg, and Su-In Lee. Explaining by removing: A unified framework for model explanation. *Journal of Machine Learning Research*, 22(209):1–90, 2021.

Jacob Devlin, Ming-Wei Chang, Kenton Lee, and Kristina Toutanova. Bert: Pre-training of deep bidirectional transformers for language understanding. *arXiv preprint arXiv:1810.04805*, 2018.

Jay DeYoung, Sarthak Jain, Nazneen Fatema Rajani, Eric Lehman, Caiming Xiong, Richard Socher, and Byron C Wallace. Eraser: A benchmark to evaluate rationalized nlp models. In *Proceedings of the 58th Annual Meeting of the Association for Computational Linguistics*, pp. 4443–4458, 2020.

Alexander Dolk, Hjalmar Davidsen, Hercules Dalianis, and Thomas Vakili. Evaluation of lime and shap in explaining automatic icd-10 classifications of swedish gastrointestinal discharge summaries. In *Scandinavian Conference on Health Informatics*, pp. 166–173, 2022.

Javier Ferrando and Marta R Costa-jussà. Attention weights in transformer nmt fail aligning words between sequences but largely explain model predictions. *arXiv preprint arXiv:2109.05853*, 2021.

Damien Garreau and Ulrike von Luxburg. Explaining the explainer: A first theoretical analysis of lime. In *International conference on artificial intelligence and statistics*, pp. 1287–1296. PMLR, 2020.

Leilani H Gilpin, David Bau, Ben Z Yuan, Ayesha Bajwa, Michael Specter, and Lalana Kagal. Explaining explanations: An overview of interpretability of machine learning. In *DSAA*, 2018.

Albert Gu and Tri Dao. Mamba: Linear-time sequence modeling with selective state spaces. *arXiv preprint arXiv:2312.00752*, 2023.

Riccardo Guidotti, Anna Monreale, Salvatore Ruggieri, Franco Turini, Fosca Giannotti, and Dino Pedreschi. A survey of methods for explaining black box models. *ACM computing surveys (CSUR)*, 51(5):1–42, 2018.

Tessa Han, Suraj Srinivas, and Himabindu Lakkaraju. Which explanation should i choose? a function approximation perspective to characterizing post hoc explanations. *Advances in Neural Information Processing Systems*, 35:5256–5268, 2022.

Yaru Hao, Li Dong, Furu Wei, and Ke Xu. Self-attention attribution: Interpreting information interactions inside transformer. In *Proceedings of the AAAI Conference on Artificial Intelligence*, volume 35, pp. 12963–12971, 2021.

Huggingface. Hugging face - models: Most downloaded sequence classification models, 2023. URL `https://huggingface.co/models?pipeline_tag=text-classification&sort=downloads`.

Katharina Jeblick, Balthasar Schachtner, Jakob Dexl, Andreas Mittermeier, Anna Theresa Stüber, Johanna Topalis, Tobias Weber, Philipp Wesp, Bastian Oliver Sabel, Jens Ricke, et al. Chatgpt makes medicine easy to swallow: an exploratory case study on simplified radiology reports. *European radiology*, pp. 1–9, 2023.

Gjergji Kasneci and Thomas Gottron. Licon: A linear weighting scheme for the contribution ofinput variables in deep artificial neural networks. In *Proceedings of the 25th ACM international on conference on information and knowledge management*, pp. 45–54, 2016.

Goro Kobayashi, Tatsuki Kuribayashi, Sho Yokoi, and Kentaro Inui. Attention is not only a weight: Analyzing transformers with vector norms. In *2020 Conference on Empirical Methods in Natural Language Processing, EMNLP 2020*, pp. 7057–7075. Association for Computational Linguistics (ACL), 2020.

Goro Kobayashi, Tatsuki Kuribayashi, Sho Yokoi, and Kentaro Inui. Feed-forward blocks control contextualization in masked language models. *arXiv preprint arXiv:2302.00456*, 2023.

Teven Le Scao, Angela Fan, Christopher Akiki, Ellie Pavlick, Suzana Ilić, Daniel Hesslow, Roman Castagné, Alexandra Sasha Luccioni, François Yvon, Matthias Gallé, et al. Bloom: A 176b-parameter open-access multilingual language model. 2023.

Scott M Lundberg and Su-In Lee. A unified approach to interpreting model predictions. *Advances in neural information processing systems*, 30, 2017.

Andrew Maas, Raymond E Daly, Peter T Pham, Dan Huang, Andrew Y Ng, and Christopher Potts. Learning word vectors for sentiment analysis. In *Proceedings of the 49th annual meeting of the association for computational linguistics: Human language technologies*, pp. 142–150, 2011.

Kit-Kay Mak, Yi-Hang Wong, and Mallikarjuna Rao Pichika. Artificial intelligence in drug discovery and development. *Drug Discovery and Evaluation: Safety and Pharmacokinetic Assays*, pp. 1–38, 2023.

Sasan Maleki, Long Tran-Thanh, Greg Hines, Talal Rahwan, and Alex Rogers. Bounding the estimation error of sampling-based shapley value approximation. *arXiv preprint arXiv:1306.4265*, 2013.

Ali Modarressi, Mohsen Fayyaz, Yadollah Yaghoobzadeh, and Mohammad Taher Pilehvar. Globenc: Quantifying global token attribution by incorporating the whole encoder layer in transformers. In *Proceedings of the 2022 Conference of the North American Chapter of the Association for Computational Linguistics: Human Language Technologies*, pp. 258–271, 2022.

Ali Modarressi, Mohsen Fayyaz, Ehsan Aghazadeh, Yadollah Yaghoobzadeh, and Mohammad Taher Pilehvar. DecompX: Explaining transformers decisions by propagating token decomposition. In *Proceedings of the 61st Annual Meeting of the Association for Computational Linguistics (Volume 1: Long Papers)*, pp. 2649–2664, 2023.

Christoph Molnar. *Interpretable Machine Learning*. 2019.

Meike Nauta, Jan Trienes, Shreyasi Pathak, Elisa Nguyen, Michelle Peters, Yasmin Schmitt, Jörg Schlötterer, Maurice Van Keulen, and Christin Seifert. From anecdotal evidence to quantitative evaluation methods: A systematic review on evaluating explainable ai. *ACM Computing Surveys*, 55(13s):1–42, 2023.

Yao Qiang, Deng Pan, Chengyin Li, Xin Li, Rhongho Jang, and Dongxiao Zhu. Attcat: Explaining transformers via attentive class activation tokens. *Advances in Neural Information Processing Systems*, 35: 5052–5064, 2022.

Alec Radford, Karthik Narasimhan, Tim Salimans, Ilya Sutskever, et al. Improving language understanding by generative pre-training. 2018.

Alec Radford, Jeffrey Wu, Rewon Child, David Luan, Dario Amodei, Ilya Sutskever, et al. Language models are unsupervised multitask learners. *OpenAI blog*, 1(8):9, 2019.

Marco Tulio Ribeiro, Sameer Singh, and Carlos Guestrin. " why should i trust you?" explaining the predictions of any classifier. In *Proceedings of the 22nd ACM SIGKDD international conference on knowledge discovery and data mining*, pp. 1135–1144, 2016.

Yao Rong, Tobias Leemann, Vadim Borisov, Gjergji Kasneci, and Enkelejda Kasneci. A consistent and efficient evaluation strategy for attribution methods. In *International Conference on Machine Learning*, pp. 18770–18795. PMLR, 2022.

Yao Rong, Tobias Leemann, Thai-Trang Nguyen, Lisa Fiedler, Peizhu Qian, Vaibhav Unhelkar, Tina Seidel, Gjergji Kasneci, and Enkelejda Kasneci. Towards human-centered explainable ai: A survey of user studies for model explanations. *IEEE Transactions on Pattern Analysis and Machine Intelligence*, 2023.

Victor Sanh, Lysandre Debut, Julien Chaumond, and Thomas Wolf. Distilbert, a distilled version of bert: smaller, faster, cheaper and lighter. *arXiv preprint arXiv:1910.01108*, 2019.

Miriam Schirmer, Isaac Misael Olguín Nolasco, Edoardo Mosca, Shanshan Xu, and Jürgen Pfeffer. Uncovering trauma in genocide tribunals: An nlp approach using the genocide transcript corpus. In *Proceedings of the Nineteenth International Conference on Artificial Intelligence and Law*, pp. 257–266, 2023.

Cansu Sen, Thomas Hartvigsen, Biao Yin, Xiangnan Kong, and Elke Rundensteiner. Human attention maps for text classification: Do humans and neural networks focus on the same words? In *Proceedings of the 58th annual meeting of the association for computational linguistics*, pp. 4596–4608, 2020.

Avanti Shrikumar, Peyton Greenside, and Anshul Kundaje. Learning important features through propagating activation differences. In *International conference on machine learning*, pp. 3145–3153. PMLR, 2017.

Karen Simonyan, Andrea Vedaldi, and Andrew Zisserman. Deep inside convolutional networks: Visualising image classification models and saliency maps. *arXiv preprint arXiv:1312.6034*, 2013.

Daniel Smilkov, Nikhil Thorat, Been Kim, Fernanda Viégas, and Martin Wattenberg. Smoothgrad: removing noise by adding noise. *arXiv preprint arXiv:1706.03825*, 2017.

Tianli Sun, Haonan Chen, Yuping Qiu, and Cairong Zhao. Efficient shapley values calculation for transformer explainability. In *Asian Conference on Pattern Recognition*, pp. 54–67. Springer, 2023.

Mukund Sundararajan, Ankur Taly, and Qiqi Yan. Axiomatic attribution for deep networks. In *International conference on machine learning*, pp. 3319–3328. PMLR, 2017.

Mateusz Szczepański, Marek Pawlicki, Rafał Kozik, and Michał Choraś. New explainability method for bert-based model in fake news detection. *Scientific reports*, 11(1):23705, 2021.

Richard Tomsett, Dan Harborne, Supriyo Chakraborty, Prudhvi Gurram, and Alun Preece. Sanity checks for saliency metrics. In *Proceedings of the AAAI Conference on Artificial Intelligence*, volume 34, pp. 6021–6029, 2020.

Hugo Touvron, Louis Martin, Kevin Stone, Peter Albert, Amjad Almahairi, Yasmine Babaei, Nikolay Bashlykov, Soumya Batra, Prajjwal Bhargava, Shruti Bhosale, et al. Llama 2: Open foundation and fine-tuned chat models. *arXiv preprint arXiv:2307.09288*, 2023.

Ashish Vaswani, Noam Shazeer, Niki Parmar, Jakob Uszkoreit, Llion Jones, Aidan N Gomez, Łukasz Kaiser, and Illia Polosukhin. Attention is all you need. *Advances in neural information processing systems*, 30, 2017.

Shawn Xu, Subhashini Venugopalan, and Mukund Sundararajan. Attribution in scale and space. In *Proceedings of the IEEE/CVF Conference on Computer Vision and Pattern Recognition*, pp. 9680–9689, 2020.

Sen Yang, Shujian Huang, Wei Zou, Jianbing Zhang, Xinyu Dai, and Jiajun Chen. Local interpretation of transformer based on linear decomposition. In *Proceedings of the 61st Annual Meeting of the Association for Computational Linguistics (Volume 1: Long Papers)*, pp. 10270–10287, 2023.

Chih-Kuan Yeh, Cheng-Yu Hsieh, Arun Suggala, David I Inouye, and Pradeep K Ravikumar. On the (in) fidelity and sensitivity of explanations. *Advances in neural information processing systems*, 32, 2019.

Ailing Zeng, Muxi Chen, Lei Zhang, and Qiang Xu. Are transformers effective for time series forecasting? In *Proceedings of the AAAI conference on artificial intelligence*, volume 37, pp. 11121–11128, 2023.

Zihan Zhou, Mingxuan Sun, and Jianhua Chen. A model-agnostic approach for explaining the predictions on clustered data. In *2019 IEEE international conference on data mining (ICDM)*, pp. 1528–1533. IEEE, 2019.

A Motivation: Failure Cases For Model Recovery

We provide another motivational example that shows a failure case of current explanation methods on transformer architectures. In this example we test the recovery property for a linear model. We create a synthetic dataset where each word in a sequence $\boldsymbol{t}$ has a linear contribution to the log-odds score, formalized by

$$\log \frac{p(y=1|\boldsymbol{t})}{p(y=0|\boldsymbol{t})} = F([t_1, t_2, \ldots, t_{|\boldsymbol{t}|}]) = b + \sum_{i=1}^{|\boldsymbol{t}|} w(t_i). \tag{6}$$

We create a dataset of 10 words (cf. Table 3) and train transformer models on samples from this dataset. We subsequently create sequences that repeatedly contain a single token τ (in this case, τ="perfect"), pass them through the transformers, and use Shapley values (approximated by Kernel-Shap) to explain their output. The result is visualized in Figure 7, and shows that a fully connected model (two-layer, 400 hidden units, ReLU) recovers the correct scores, whereas trainsformer models fail to reflect the true relationship. This shows that explanation methods that are explicitly or implicitly based on additive models lose their ability to recover the true data-generating process when transformer models are explained.

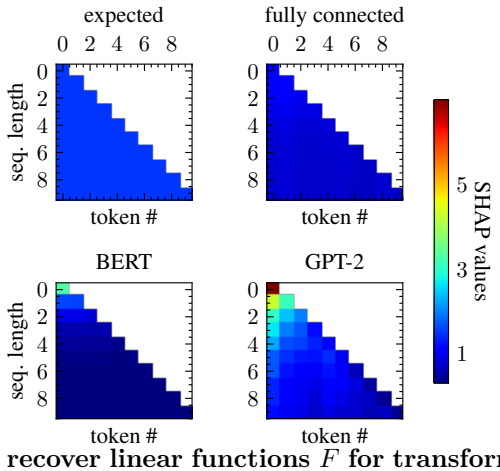

Figure 7: **SHAP values do not recover linear functions F for transformers.** We compute SHAP values for token sequences that repeatedly contain a single token τ with a ground truth score of 1.5 (i.e., $F([\tau])$=1.5, $F([\tau, \tau])$=3.0, ...) such that the ground truth attributions should yield 1.5 independent of the sequence length. While this approximately holds true for a fully connected model, BERT and GPT-2 systematically overestimate the importance for short sequences and underestimate it for longer ones.

B Proofs

B.1 Formalization of the transformer

Many popular LLMs follow the transformer architecture introduced by Vaswani et al. (2017) with only minor modifications. We will introduce the most relevant building blocks of the architecture in this section. A schematic overview of the architecture is visualized in Figure 2. Let us denote the input embeddings for Layer $l \in 1, \ldots L$ by $\boldsymbol{H}^{(l-1)} = [\boldsymbol{h}_1^{(l-1)}, \ldots, \boldsymbol{h}_{|\boldsymbol{t}|}^{(l-1)}]^\top \in \mathbb{R}^{|\boldsymbol{t}| \times d}$, where a single line $\boldsymbol{h}_i$ contains the embedding for token i. The input embeddings of the first layer consist of the token embeddings, i.e., $\boldsymbol{H}^{(0)} = \boldsymbol{E}$. At the core of the architecture lies the attention head. For each token, a *query*, *key*, and a *value* vector are computed

by applying an affine-linear transform. In matrix notation this can be written as

$$\boldsymbol{Q}^{(l)} = \boldsymbol{H}^{(l-1)}\boldsymbol{W}_Q^{(l)} + \mathbf{1}_{|\boldsymbol{t}|}\boldsymbol{b}_Q^{(l)\top}, \tag{7}$$

$$\boldsymbol{K}^{(l)} = \boldsymbol{H}^{(l-1)}\boldsymbol{W}_K^{(l)} + \mathbf{1}_{|\boldsymbol{t}|}\boldsymbol{b}_K^{(l)\top}, \tag{8}$$

$$\boldsymbol{V}^{(l)} = \boldsymbol{H}^{(l-1)}\boldsymbol{W}_V^{(l)} + \mathbf{1}_{|\boldsymbol{t}|}\boldsymbol{b}_V^{(l)\top}, \tag{9}$$

where $\mathbf{1}_{|\boldsymbol{t}|} \in \mathbb{R}^{|\boldsymbol{t}|}$ denotes a vector of ones of length $|\boldsymbol{t}|$, $\boldsymbol{b}_Q^{(l)}, \boldsymbol{b}_V^{(l)}, \boldsymbol{b}_K^{(l)} \in \mathbb{R}^{d_h}$, $\boldsymbol{W}_Q^{(l)}, \boldsymbol{W}_K^{(l)}, \boldsymbol{W}_V^{(l)} \in \mathbb{R}^{d \times d_h}$, are trainable parameters and d_h denotes the dimension of the attention head.[2] Keys and queries are projected onto each other and normalized by a row-wise softmax operation,

$$\boldsymbol{A}^{(l)} = \text{rowsoftmax}\left(\frac{\boldsymbol{Q}^{(l)}\boldsymbol{K}^{(l)\top}}{\sqrt{d_k}}\right). \tag{10}$$

This results in the attention matrix $\boldsymbol{A}^{(l)} \in \mathbb{R}^{|t| \times |t|}$, where row i indicates how much the other tokens will contribute to its output embedding. To compute output embeddings, we obtain attention outputs $\boldsymbol{s}_i$,

$$\boldsymbol{S} = [\boldsymbol{s}_1, \ldots, \boldsymbol{s}_{|\boldsymbol{t}|}]^\top = \boldsymbol{A}^{(l)}\boldsymbol{V}^{(l)}. \tag{11}$$

Note that an attention output can be computed as $\boldsymbol{s}_i = \sum_{j=1}^{|\boldsymbol{t}|} a_{ij}\boldsymbol{v}_j$, where $\boldsymbol{v}_j$ denotes the value vector in the line corresponding to token j in $\boldsymbol{V} = [\boldsymbol{v}_1, \ldots, \boldsymbol{v}_{|\boldsymbol{t}|}]^\top$ and $a_{ij} = \boldsymbol{A}_{i,j}^{(l)}$. The final $\boldsymbol{s}_i$ are projected back to the original dimension d by some projection operator $P : \mathbb{R}^{d_h} \to \mathbb{R}^d$ before they are added to the corresponding input embedding $\boldsymbol{h}_i^{(l-1)}$ due to the skip-connections. The sum is then transformed by a nonlinear function that we denote by $\text{ffn} : \mathbb{R}^d \to \mathbb{R}^d$. In summary, we obtain the output for the layer, $\boldsymbol{h}_i^{(l)}$, with

$$\boldsymbol{h}_i^{(l)} = \text{ffn}_l(\boldsymbol{h}_i^{(l-1)} + \boldsymbol{P}(\boldsymbol{s}_i)). \tag{12}$$

This procedure is repeated iteratively for layers $1, \ldots, L$ such that we finally arrive at output embeddings $\boldsymbol{H}^{(L)}$. To perform classification, a classification head $\text{cls} : \mathbb{R}^d \to \mathbb{R}^{|\mathcal{V}|}$ is put on top of a token at classification index r (how this token is chosen depends on the architecture, common choices include $r \in \{1, |\boldsymbol{t}|\}$), such that we get the final logit output $\boldsymbol{l} = \text{cls}\left(\boldsymbol{h}_r^{(L)}\right)$. The logit output is transformed to a probability vector via another softmax operation. Note that in the two-class case, we obtain the log-odds $F(\boldsymbol{t})$ by taking the difference (Δ) between logits

$$F(\boldsymbol{t}) \coloneqq \log\frac{p(y=1|\boldsymbol{t})}{p(y=0|\boldsymbol{t})} = \Delta(\boldsymbol{l}) = \boldsymbol{l}_1 - \boldsymbol{l}_0. \tag{13}$$

B.2 Proof of Proposition 4.1

Proposition B.1 (Proposition 4.1 in the main paper)**.** *Let $\mathcal{V}$ be a vocabulary and $C \geq 2, C \in \mathbb{N}$ be a maximum sequence length (context window). Let $w_i : \mathcal{V} \to \mathbb{R}, \forall i \in 1, ..., C$ be any mapping that assigns a token encountered at position i a numerical score including at least one token $\tau \in \mathcal{V}$ with non-zero weight $w_i(\tau) \neq 0$ for some $i \in 2, \ldots, C$. Let $b \in \mathbb{R}$ be an arbitrary offset. Then, there exists no parametrization of the encoder or decoder single-layer transformer F such that for every sequence $\boldsymbol{t} = [t_1, t_2, \ldots, t_{|\boldsymbol{t}|}]$ with length $1 \leq |\boldsymbol{t}| \leq C$, the output of the transformer network is equivalent to*

$$F([t_1, t_2, \ldots, t_{|\boldsymbol{t}|}]) = b + \sum_{i=1}^{|\boldsymbol{t}|} w_i(t_i). \tag{14}$$

Proof. We show the statement in the theorem by contradiction. Consider the token, $\tau \in \mathcal{V}$, for which $w_j(\tau) \neq 0$ for some token index $j \geq 2$ which exists by the condition in the theorem. We now consider

[2]We only formalize one attention head here, but consider the analogous caae of multiple heads in our formal proofs.

sequences of length k of the form $\boldsymbol{t}_k = [\underbrace{\tau, \ldots, \tau}_{\text{repeat } k \text{ times}}]$ for $k = 1, \ldots, C$. For example, we have $\boldsymbol{t}_1 = [\tau]$, $\boldsymbol{t}_2 = [\tau, \tau]$, etc. The output of the transformer is given by

$$F(\boldsymbol{t}) = g\left(\boldsymbol{h}_r^{(0)}, \sum_{j=1}^{|\boldsymbol{t}|} a_{rj}\boldsymbol{v}_j\right) = g\left(\boldsymbol{e}(\tau), \sum_{j=1}^{|\boldsymbol{t}|} \alpha_{rj}\boldsymbol{v}_j\right), \tag{15}$$

where r is the token index on which the classification head is placed. Note that with $r = |\boldsymbol{t}|$ for the decoder architecture, the sum always goes up to $|\boldsymbol{t}|$ (for the encoder architecture this is always true). As all tokens in the sequence have a value of τ, we obtain $\boldsymbol{h}_r^{(0)} = \boldsymbol{e}(t_r) = \boldsymbol{e}(\tau)$. The first input to the final part will thus be equal for all sequences $\boldsymbol{t}_k$. We will now show that the second part will also be equal.

We compute the value, key, and query vectors for τ. $\boldsymbol{v}, \boldsymbol{k}, \boldsymbol{q} \in \mathbb{R}^{d_h}$ correspond to one line in the respective key, query and value matrices. As the inputs are identical and we omit positional embeddings in this proof, all lines are identical in the matrices. This results in

$$\boldsymbol{v} = \boldsymbol{W}_V^\top \boldsymbol{e}(\tau) + \boldsymbol{b}_V \tag{16}$$

$$\boldsymbol{k} = \boldsymbol{W}_K^\top \boldsymbol{e}(\tau) + \boldsymbol{b}_K \tag{17}$$

$$\boldsymbol{q} = \boldsymbol{W}_Q^\top \boldsymbol{e}(\tau) + \boldsymbol{b}_Q \tag{18}$$

We omit the layer indices for simplicity. As pre-softmax attention scores (product of key and value vector), we obtain $s = \boldsymbol{q}^\top \boldsymbol{k}/\sqrt{d_k}$. Subsequently, the softmax computation will be performed over the entire sequence, resulting in

$$\boldsymbol{\alpha}_r = \text{softmax}([\underbrace{s, \ldots, s}_{k \text{ times}}]) = \left[\frac{\exp(s)}{k\exp(s)}\right] \tag{19}$$

$$= \left[\underbrace{\frac{1}{k}, \ldots, \frac{1}{k}}_{k \text{ times}}\right] \tag{20}$$

The second input $\sum_{j=1}^{|\boldsymbol{t}|} \alpha_{rj}\boldsymbol{v}_j$ to the feed-forward part is given by

$$\sum_{j=1}^{|\boldsymbol{t}|} \alpha_{rj}\boldsymbol{v}_j = \sum_{j=1}^{k} \alpha_{rj}\boldsymbol{v}_j = \sum_{j=1}^{k} \frac{1}{k}\boldsymbol{v} = \boldsymbol{v}, \tag{21}$$

as α_{rj} and $\boldsymbol{v}$ are independent of the token index j. We observe that the total input to final part g is independent of k in its entirety, as the first input $\boldsymbol{e}(\tau)$ is independent of k and the second input is independent of k as well. As g is a deterministic function, also the log-odds output will be the same for all input sequences $\boldsymbol{t}_k$ and be independent of k. By the condition we have a non-zero weight $w_j(\tau) \neq 0$ for some $j \geq 2$. In this case, there are two sequences $\boldsymbol{t}_{j-1}$ (length $j-1$) and $\boldsymbol{t}_j$ (length j) consisting of only token τ, where the outputs of the GAM follow

$$f_{\text{GAM}}(\boldsymbol{t}_j) = b + \sum_{i=1}^{j} w_i(\tau) \tag{22}$$

$$= b + \sum_{i=1}^{j-1} w_i(\tau) + w_j(\tau) \tag{23}$$

$$= f_{\text{GAM}}(\boldsymbol{t}_{j-1}) + w_j(\tau) \tag{24}$$

As we suppose $w_j(\tau) \neq 0$, it must be that $f_{\text{GAM}}(\boldsymbol{t}_j) \neq f_{\text{GAM}}(\boldsymbol{t}_{j-1})$ which is a contradiction, with the output being equal for all sequence lengths.

Multi-head attention. In the case of multiple heads, we have

$$F(\boldsymbol{t}) = \Delta\left(\text{cls}(\boldsymbol{h}_r^{(1)})\right) \tag{25}$$

$$= \Delta\left(\text{cls}\left(\text{ffn}(\boldsymbol{h}_r^{(0)} + \boldsymbol{P}_{h=1}(\boldsymbol{s}_r^{h=1}) + \boldsymbol{P}_{h=2}(\boldsymbol{s}_r^{h=2}) + \ldots + \boldsymbol{P}_{h=1}(\boldsymbol{s}_r^{h=H}))\right)\right) \tag{26}$$

$$= g(\boldsymbol{h}_r^{(0)}, \boldsymbol{s}_r^{h=1}, \ldots, \boldsymbol{s}_r^{h=H}) \tag{27}$$

As before, we can make the same argument, if we show that all inputs to g are the same. This is straightforward, as we can extend the argument made for one head for every head, because none of the head can differentiate between the sequence lengths. The first input will still correspond to $\boldsymbol{h}_r^{(0)} = \boldsymbol{e}(\tau)$, which results in the same contradiction. □

B.3 Corollary: Transformers cannot represent linear models

Corollary B.2 (Transformers cannot represent linear models)**.** *Let the context window be $C > 2$ and suppose the same model as in Proposition 4.1. Let $w : \mathcal{V} \to \mathbb{R}$ be any weighting function that is independent of the token position with $w(\tau) \neq 0$ where for at least one token $\tau \in \mathcal{V}$. Then, the single layer transformer cannot represent the linear model*

$$F([t_1, t_2, \ldots, t_N]) = b + \sum_{i=1}^{N} w(t_i). \tag{28}$$

Proof. This can be seen by setting $w_i \equiv w$ for every i in Proposition 4.1. With $w(\tau) \neq 0$, the condition from Proposition 4.1, i.e., having one w_i with $w_i(\tau) \neq 0$ for $i \geq 2$ is fulfilled as well such that the result of the proposition as well. □

This statement has a strong implication on the capabilities of transformers as it shows that they struggle to learn linear models.

B.4 Proof of Corollary 4.3

Corollary B.3 (Corollary 4.2 in the main paper)**.** *Under the same conditions as in Proposition 4.1, a stack of multiple transformer blocks as in the model F neither has a parametrization sufficient to represent the linear model.*

Proof. We show the result by induction, with the help of a lemma.

Lemma: Suppose a set S of sequences. If (1) for every sequence $\boldsymbol{t} \in S$ the input matrix $\boldsymbol{H}^{(l)} = [\boldsymbol{h}_1^{(l)}, \ldots, \boldsymbol{h}_{|\boldsymbol{t}|}^{(l)}]$ will consist of input embeddings that are identical for each token i, and (2) single input embeddings also have the same value for every sequence $\boldsymbol{t} \in S$, in the output $\boldsymbol{H}^{(l+1)}$ (1) the output embeddings will be identical for all tokens i and (2) they will have equal value for all the sequences $\boldsymbol{t} \in S$ considered before.

For the encoder-only architecture, the proof from Proposition 4.1 holds analogously for each token output embedding (in the previous proof, we only considered the output embedding at the classification token r). Without restating the full proof the main steps consist of

- showing the attention to be equally distributed across tokens, i.e., $\alpha_{ij} = 1/|\boldsymbol{t}|$
- showing the value vectors $\boldsymbol{v}_i$ to be equal because they only depend on the input embeddings which are equal
- concluding that the output will be equal regardless of the number of inputs

This shows that for each sequence $\boldsymbol{t} \in S$, the output at token i remains constant. To show that all tokens i result in the same output, we observe that the the only dependence of the input token to the output is through the query, which however is also equivalent if we have the same inputs.

For the decoder-only architecture, for token i, the attention weights are taken only up to index i resulting in a weight of $\frac{1}{i}$ for each previous token and a weight of 0 (masked) for subsequent ones. However, with the sum also being equal to 1 and the value vectors being equivalent, there is no difference in the outcome. This proves the lemma.

Having shown this lemma, we consider a set S of two sequences $S = \{\boldsymbol{t}_{j-1}, \boldsymbol{t}_j\}$ where $\boldsymbol{k}_{j-1}$ contains $j-1$ repetitions of token τ and $\boldsymbol{t}_j$ contains j repetitions of token τ. We chose $j \geq 2, \tau$ such that $w_j(\tau) \neq 0$, which is possible by the conditions of the theorem. We observe that for $\boldsymbol{H}^{(0)}$, the embeddings are equal for each token and their value is the same for both sequences. We then apply the lemma for layers $1, \ldots, L$, resulting in the output embeddings of $\boldsymbol{H}^{(L)}$ being equal for each token, and most importantly identical for $\boldsymbol{t}_{j-1}$ and $\boldsymbol{t}_j$. As we perform the classification by $F(\boldsymbol{t}) = \Delta\left(\text{cls}\left(\boldsymbol{h}_r^{(L)}\right)\right)$, this output will also not change with the sequence length. This result can be used to construct the same contradiction as in the proof of Proposition 4.1. □

B.5 Proof of Proposition 5.1

Proposition B.4 (Transformers can easily fit SLALOM models)**.** *For any mapping s, v and a transformer with an embedding size $d, d_h \geq 3$, there exists a parameterization of the transformer to reflect the SLALOM model in Equation* (4)*.*

Proof. We can prove the theorem by constructing a weight setup to reflect this mapping. We let the embedding $\boldsymbol{e}(\tau)$ be given by

$$\boldsymbol{e}(\tau) = [s(\tau), v(\tau), 0, 0, \ldots, 0]. \tag{29}$$

We then set the key mapping matrix K to be

$$\boldsymbol{W}_k = \boldsymbol{0} \tag{30}$$
$$\boldsymbol{b}_k = [1, 0, \ldots, 0]. \tag{31}$$

such that we have

$$\boldsymbol{W}_k \boldsymbol{e}(\tau) + \boldsymbol{b}_k = [1, 0, \ldots, 0]. \tag{32}$$

For the query mapping we can use

$$\boldsymbol{W}_q = \boldsymbol{I} \tag{33}$$
$$\boldsymbol{b}_q = \boldsymbol{0} \tag{34}$$

such that

$$\boldsymbol{W}_v \boldsymbol{e}(\tau) + \boldsymbol{b}_v = [s(\tau), v(\tau), 0, \ldots, 0]. \tag{35}$$

This results in the non-normalized attention scores for query $\tau \in \mathcal{V}$ and key $\theta \in \mathcal{V}$

$$a(t_i, t_j) = (\boldsymbol{W}_q \boldsymbol{e}(t_i) + \boldsymbol{b}_q)^\top (\boldsymbol{W}_k \boldsymbol{e}(t_j) + \boldsymbol{b}_k) = s(t_j) \tag{36}$$

We see that regardless of the query token, the pre-softmax score will be $s(\theta)$. For the value scores, we perform a similar transform with

$$\boldsymbol{W}_v = \text{diag}\left([0, 1, 0, \ldots, 0]\right) \tag{37}$$
$$\boldsymbol{b}_v = \boldsymbol{0} \tag{38}$$

such that

$$\boldsymbol{v}_i = \boldsymbol{W}_v \boldsymbol{e}(t_i) + \boldsymbol{b}_v = [0, 0, v(t_i), 0, \ldots, 0]. \tag{39}$$

We then obtain

$$\boldsymbol{s}_r = \sum_{t_i \in \boldsymbol{t}} a_{ri} \boldsymbol{v}_i = \sum_{t_i \in \boldsymbol{t}} \text{softmax}_i[s(t_1), \ldots, s(t_{|\boldsymbol{t}|})] \boldsymbol{v}_i \tag{40}$$

$$= \left[0, 0, \sum_{t_i \in \boldsymbol{t}} \alpha_i(\boldsymbol{t}) v(t_i), \ldots, 0\right]^\top \tag{41}$$

We saw that the final output can be represented by

$$F(\boldsymbol{t}) = \Delta\left(\text{cls}\left(\text{ffn}\left(\boldsymbol{e}(t_0) + P(\boldsymbol{s}_r)\right)\right)\right) \tag{42}$$

The projection operator is linear, which can set to easily forward in input by setting $\boldsymbol{P} \equiv \boldsymbol{I}$. Due to the skip connection of the feed-forward part, we can easily transfer the second part through the first ffn part. In the classification part, we output the third component and zero by applying the final weight matrix

$$\boldsymbol{W}_{class} = \begin{bmatrix} 0 & 0 & 0 & \cdots & 0 \\ 0 & 0 & 1 & \cdots & 0 \end{bmatrix} \tag{43}$$

and a bias vector of $\mathbf{0}$.

Multiple Heads. Multiple heads can represent the pattern by choosing $P = \boldsymbol{I}$ for one head and choosing $P = \mathbf{0}$ for the other heads.

Multiple Layers. We can extend the argument to multiple layers by showing that the input vectors can just be forwarded by the transformer. This is simple by setting $\boldsymbol{P} \equiv \mathbf{0}$, the null-mapping, which can be represented by a linear operator. We then use the same classification hat as before. □

B.6 Proof of Proposition 5.2

Proposition B.5 (Proposition 5.2. in the main paper)**.** *Suppose query access to a model G that takes sequences of tokens $\boldsymbol{t}$ with lengths $|\boldsymbol{t}| \in 1, \ldots, C$ and returns the log-odds according to a non-constant SLALOM on a vocabulary $\mathcal{V}$ with unknown parameter mappings $s : \mathcal{V} \to \mathbb{R}$, $v : \mathcal{V} \to \mathbb{R}$. For $C \geq 2$, we can recover the true mappings s, v with $2|\mathcal{V}| - 1$ queries (forward passes) of F.*

Proof. We first compute $G([\tau]), \forall \tau \in \mathcal{V}$. We know that for single token sequences, all attention is on one token, i.e., $(\alpha_i = 1)$ and we thus have

$$G([\tau]) = v(\tau) \tag{44}$$

We have obtained the values scores v for each token through $|\mathcal{V}|$ forward passes. To identify the token importance scores s, we consider token sequences of length 2.

We first note that if the SLALOM is non-constant and $|\mathcal{V}| > 1$, for every token $\tau \in \mathcal{V}$, we can find another token θ for which $v(\tau) \neq v(\theta)$. This can be seen by contradiction: If this would not be the case, i.e., we cannot find a token ω with a different value $v(\omega)$, all tokens have the same value and the SLALOM would have to be constant. For $|\mathcal{V}| = 1$, SLALOM is always constant and does not fall under the conditions of the theorem.

We now select an arbitrary reference token $\theta \in \mathcal{V}$. We select another token $\hat{\theta}$ for which $v(\hat{\theta}) \neq v(\theta)$. By the previous argument such a token always exists if the SLALOM is non-constant. We now compute relative importances w.r.t. θ that we refer to as η_θ. We let $\eta_\theta(\tau) = s(\tau) - s(\theta)$ denote the difference of the importance between the importance scores of tokens $\tau, \theta \in \mathcal{V}$. We set $\eta_\theta(\theta) = 0$

We start with selecting token $\tau = \hat{\theta}$ and subsequently use each other token $\tau \neq \theta$ to perform the following steps **for each** $\tau \neq \theta$:

1. Identify reference token $\hat{\tau}$. We now have to differentiate two cases: If $v(\tau) = v(\theta)$, we select $\hat{\tau} = \hat{\theta}$ as the reference token. If $v(\tau) \neq v(\theta)$, we select $\hat{\tau} = \theta$ as the reference token. By doing so, we will always have $v(\hat{\tau}) \neq v(\tau)$.

2. Compute $G([\tau, \hat{\tau}])$. We now compute $G([\tau, \hat{\tau}])$. From the model's definition, we know that

$$\begin{aligned} G([\tau, \hat{\tau}]) =& \frac{\exp(s(\tau))}{\exp(s(\tau)) + \exp(s(\hat{\tau}))} v(\tau) && (45)\\ &+ \frac{\exp(s(\hat{\tau}))}{\exp(s(\tau)) + \exp(s(\hat{\tau}))} v(\hat{\tau}) && (46)\\ =& \frac{\exp(s(\tau))}{\exp(s(\tau)) + \exp(s(\hat{\tau}))} G([\tau]) && (47)\\ &+ \frac{\exp(s(\hat{\tau}))}{\exp(s(\tau)) + \exp(s(\theta))} G([\hat{\tau}]) && (48)\\ =& \frac{\exp(s(\tau))}{\exp(s(\tau)) + \exp(s(\hat{\tau}))} G([\tau])) && (49)\\ &+ \left(1 - \frac{\exp(s(\tau))}{\exp(s(\tau)) + \exp(s(\hat{\tau}))}\right) G([\hat{\tau}]) && (50) \end{aligned}$$

which we can rearrange to

$$G([\tau, \hat{\tau}]) - G([\hat{\tau}]) = \frac{\exp(s(\tau))}{\exp(s(\tau)) + \exp(s(\hat{\tau}))} \left(G([\tau]) - G([\hat{\tau}])\right) \tag{51}$$

and finally to

$$\frac{\exp(s(\tau))}{\exp(s(\tau)) + \exp(s(\hat{\tau}))} = \frac{G([\tau, \hat{\tau}]) - G([\hat{\tau}])}{G([\tau]) - G([\hat{\tau}])} \coloneqq g(\tau, \hat{\tau}) \tag{52}$$

and

$$\begin{aligned} \frac{1}{1 + \frac{\exp(s(\hat{\tau}))}{\exp(s(\tau))}} &= g(\tau, \hat{\tau}) && (53)\\ \Leftrightarrow \frac{1}{g(\tau, \hat{\tau})} &= 1 + \frac{\exp(s(\hat{\tau}))}{\exp(s(\tau))} && (54)\\ \Leftrightarrow \log\left(\frac{1}{g(\tau, \hat{\tau})} - 1\right) &= s(\tau) - s(\hat{\tau}) \coloneqq d(\tau, \hat{\tau}) && (55) \end{aligned}$$

This allows us to express the importance of every token $\tau \in \mathcal{V}$ relative to the base token $\hat{\tau}$.

3. Compute importance relative to θ, i.e., $\eta_\theta(\tau)$. In case we selected $\hat{\tau} = \theta$, we set $\eta_\theta(\tau) = d(\tau, \hat{\tau}) = s(\tau) - s(\theta)$. In case we selected $\hat{\tau} = \hat{\theta}$, we set

$$\eta_\theta(\tau) = d(\tau, \hat{\tau}) - d(\hat{\theta}, \theta) = s(\tau) - s(\hat{\theta}) + (s(\hat{\theta}) - s(\theta)) = s(\tau) - s(\theta) \tag{56}$$

The value of $d(\hat{\theta}, \theta)$ is already known from the first iteration of the loop, where we consider $\tau = \hat{\theta}$ (and needs to be computed only once).

Having obtained a value of $\eta_\theta(\tau)$ for each token $\tau \neq \theta$, with $|\mathcal{V}| - 1$ forward passes, we can then use the normalization in constraint to solve for $s(\theta)$ as in

$$\sum_{\tau \in \mathcal{V}} (\eta_\theta(\tau) + s(\theta)) =^! 0 \tag{57}$$

such that we obtain

$$s(\theta) = \frac{\sum_{\tau \in \mathcal{V}} \eta_\theta(\tau)}{|\mathcal{V}|} \tag{58}$$

We can plug this back in to obtain the values for all token importance scores $s(\tau) = s(\theta) + \eta_\theta(\tau)$. We have thus computed the mappings s and v in $2|\mathcal{V}| - 1$ forward passes, which completes the proof. □

B.7 Relating SLALOM to other attribution techniques.

Local Linear Attribution Scores. We can consider the following weighted model:

$$F(\boldsymbol{\lambda}) = \frac{\sum_{t_i \in \boldsymbol{t}} \lambda_i \exp(s(t_i)) v(t_i)}{\sum_{t_i \in \boldsymbol{t}} \lambda_i \exp(s(t_i))} \tag{59}$$

where $\lambda_i = 1$ if a token is present and $\lambda_i = 0$ if it is absent. We observe that setting $\lambda_i = 0$ has the desired effect of making the output of the weighted model equivalent to that of the unweighted SLALOM on a sequence without this token.

Taking the derivative at $\boldsymbol{\lambda} = \mathbf{1}$ results in

$$\frac{\partial F}{\partial \lambda_i} = \frac{\exp(s(t_i)) v(t_i) \left(\sum_{t_j \in \boldsymbol{t}, j \neq i} \lambda_j \exp(s(t_j)) \right)}{\left(\sum_{t_j \in \boldsymbol{t}} \lambda_j \exp(s(t_j)) \right)^2} \tag{60}$$

$$- \frac{\exp(s(t_i)) \left(\sum_{t_j \in \boldsymbol{t}, j \neq i} \lambda_j \exp(s(t_j)) v(t_j) \right)}{\left(\sum_{t_j \in \boldsymbol{t}} \lambda_j \exp(s(t_j)) \right)^2} \tag{61}$$

Plugging in $\boldsymbol{\lambda} = \mathbf{1}$, and using $\alpha_i(\boldsymbol{t}) = \frac{\exp(s(t_i))}{\sum_{t_j \in \boldsymbol{t}} \lambda_j \exp(s(t_j))}$ we obtain

$$\left. \frac{\partial F}{\partial \lambda_i} \right|_{\boldsymbol{\lambda}=\mathbf{1}} = \alpha_i \left(v(t_i)(1 - \alpha_i(\boldsymbol{t})) - (F(\mathbf{1}) - \alpha_i v(t_i)) \right) \tag{62}$$

$$= \alpha_i \left((v(t_i) - \alpha_i v(t_i))) - (F(\mathbf{1}) - \alpha_i v(t_i)) \right) \tag{63}$$

$$= \alpha_i \left(v(t_i) - F(\mathbf{1}) \right) \tag{64}$$

Noting that $\alpha_i = \frac{\exp(s(t_i))}{R}$, where R and $F(\mathbf{1})$ are independent of i, we obtain

$$\left. \frac{\partial F}{\partial \lambda_i} \right|_{\boldsymbol{\lambda}=\mathbf{1}} \propto v(t_i) \exp(s(t_i)), \tag{65}$$

which can be used to rank tokens according the locally linear attributions. We refer to this expression as linearized SLALOM scores ("lin").

Shapley Values. We can convert SLALOM scores to Shapley values $\phi(i)$ using the explicit formula:

$$\phi(i) = \frac{1}{n} \sum_{S \subset [N] \setminus \{i\}} \binom{n-1}{|S|} (F(S \cup \{i\}) - F(S)) \tag{66}$$

$$= \frac{1}{n} \sum_{S \subset [N] \setminus \{i\}} \binom{n-1}{|S|} \left(F(S \cup \{i\}) - \frac{F(S \cup \{i\}) - \alpha_i v_i}{1 - \alpha_i} \right) \tag{67}$$

$$= \frac{1}{n} \sum_{S \subset [N] \setminus \{i\}} \binom{n-1}{|S|} \left(\frac{\alpha_i (v_i - F(S \cup \{i\}))}{1 - \alpha_i} \right) \tag{68}$$

$$\left(\frac{\alpha_i (v_i - F(\mathbf{1}))}{1 - \alpha_i} \right) \tag{69}$$

However, computing this sum remains usually intractable, as the number of coalitions grows exponentially. We can resort to common sampling approaches (Castro et al., 2009; Maleki et al., 2013) to approximate the sum.

C Additional Dicucssion and Intuition

C.1 Generalization to multi-class problems

We can imagine the following generalizing SLALOM to multi class problems as follows: Suppose we have an importance mapping $s : \mathcal{V} \to \mathbb{R}$ that still maps each token to an importance score. However, we now introduce a value score mapping $v_c : \mathcal{V} \to \mathbb{R}$ for each class $c \in \mathcal{Y}$. Addtionally to requiring

$$\sum_{\tau \in \mathcal{V}} s(\tau) = 0. \tag{70}$$

we now require

$$\sum_{c \in \mathcal{Y}} v_c(\tau) = 0, \forall \tau \in \mathcal{V} \tag{71}$$

For an input sequence $\boldsymbol{t}$, the SLALOM model then computes

$$F_c(\boldsymbol{t}) = \log \frac{p(y=1|\boldsymbol{t})}{p(y=0|\boldsymbol{t})} = \sum_{\tau_i \in \boldsymbol{t}} \alpha_i(\boldsymbol{t}) v_c(t_i), \tag{72}$$

The posterior probabilities can be computed by performing a softmax operation over the F-scores, as in

$$p(y=c|\boldsymbol{t}) = \frac{\exp(F_c(\boldsymbol{t}))}{\sum_{c' \in \mathcal{Y}} \exp(F_{c'}(\boldsymbol{t}))} \tag{73}$$

We observe that this model has $\big(|\mathcal{Y}|-1\big)|\mathcal{V}|-1$ free parameters (for the two-class problem, this yields $2|\mathcal{V}|-1$ as before) and can be fitted and deployed as the two-class SLALOM without major ramifications.

C.2 Practical Considerations

Our theoretical model contains slight deviations from real-world transformers to make it amendable to theoretical analysis. To represent token order, common architectures use positional embeddings, tying the embedding vectors to the token position i. The behavior that we show in this work's analysis does however also govern transformers with positional embeddings for the following reason: While the positional embeddings could be used by the non-linear ffn part to differentiate sequences of different length in theory, our proofs show that to represent the linear model, the softmax operation must be inverted for any input sequence. This is a highly nonlinear operation and the number of possible sequences grows exponentially at a rate of $|\mathcal{V}|^C$ with the context length C. Learning-theoretic considerations (e.g., Bartlett et al., 1998) show that the number of input-output pairs the two-layer networks deployed can maximally represent is bounded by $\mathcal{O}\left(dn_{\text{hidden}} \log(dn_{\text{hidden}})\right)$, which is small ($d$=786, n_{hidden}=3072 for BERT) in contrast to the number of sequences ($C = 1024$, $|\mathcal{V}| \approx 3 \times 10^4$). We conclude that the inversion is therefore impossible for realistic setups and positional embeddings can be neglected, which is confirmed by our empirical findings.

Common models such as BERT also use a special token referred to as `CLS`-token where the classification head is placed on. In this work, we consider the `CLS` token just as a standard token in our analysis. In our empirical sections, we always append the `CLS` token as mandated by the architecture to make the sequences valid model inputs.

D Algorithm: Local SLALOM approximation

We propose two algorithms to compute local explanations for a sequence $\boldsymbol{t} = [t_1, \ldots, t_{|\boldsymbol{t}|}]$ with SLALOM scores. In particular, we use the Mean-Squared-Error (MSE) to fit SLALOM on modified sequences consisting of the individual tokens in the original sequence $\boldsymbol{t}$. To speed up the fitting we can sample a large collection of samples offline before the optimization.

D.1 Efficiently fitting SLALOM with SGD

For the efficient implementation SLALOM-`eff` given in Algorithm 1 we sample minibatches from this collection in each step and perform SGD steps on them. We perform this optimization using $b = 5000$ samples in this work. We use sequences of $n = 2$ random tokens from the sample for SLALOM-`eff`, making the forward passes through the model highly efficient.

D.2 Fitting SLALOM through iterative optimization

For the high-fidelity implementation SLALOM-`fidel` (Algorithm 2) we first use a different set of sequences and model scores to fit the surrogate: We delete up to 5 tokens from the original sequence randomly to create the estimation dataset (similar to LIME). The fitting algorithm optimized for maximum fidelity uses an iterative optimization scheme to fit SLALOM models. It works by iteratively fitting $\boldsymbol{v}$ and $\boldsymbol{s}$ to the dataset obtained. Denote by $\boldsymbol{f} \in \mathbb{R}^b$ the model scores obtained for the b input sequences $\boldsymbol{t}_i, i = 1...b$. As the SLALOM model in Equation (4) is a linear combination of the values score weighted by the normalized importance score, we can set up a matrix $\boldsymbol{A}$, where element $\boldsymbol{a}_{i,j} = \frac{\exp(s(t_i))}{\sum_{t_j \in \boldsymbol{t}_i} \exp(s(t_j))}$ provides the normalized importance for a given $\boldsymbol{s}$. We solve

$$\min_{\boldsymbol{v}} (\boldsymbol{A}\boldsymbol{v} - \boldsymbol{f})^\top (\boldsymbol{A}\boldsymbol{v} - \boldsymbol{f}), \tag{74}$$

for $\boldsymbol{v}$, which is a linear ordinary least squared problem that can be solved through the normal equation. This results in the optimal $\boldsymbol{v}$ for the given $\boldsymbol{s}$. In a second step, we keep $\boldsymbol{v}$ fixed and find better $\boldsymbol{s}$ scores. We can reformulate the equations for the samples as

$$\sum_{t_j \in \boldsymbol{t}_i} \exp(s(t_j)) v(t_j) = \left(\sum_{t_j \in \boldsymbol{t}_i} \exp(s(t_j)) \right) \boldsymbol{f}_i \tag{75}$$

$$\Leftrightarrow \sum_{t_j \in \boldsymbol{t}_i} \underbrace{\exp(s(t_j))}_{\bar{\boldsymbol{s}}_j} \underbrace{(v(t_j) - \boldsymbol{f}_i)}_{e_{i,j}} = 0. \tag{76}$$

This problem can be written with a vector $\bar{\boldsymbol{s}} \in \mathbb{R}^{|\mathcal{V}|}$ and a matrix $\boldsymbol{E} \in \mathbb{R}^{b \times |\mathcal{V}|}$ and results in an optimization problem

$$\min_{\bar{\boldsymbol{s}}} (\boldsymbol{E}\bar{\boldsymbol{s}})^\top (\boldsymbol{E}\bar{\boldsymbol{s}}), \tag{77}$$

$$\text{s.t. } \hat{\boldsymbol{s}} \geq \boldsymbol{0} \tag{78}$$

$$\|\hat{\boldsymbol{s}}\|_1 \geq |\mathcal{V}| \tag{79}$$

The conditions ensure that we can obtain the original $\boldsymbol{s}$-scores as $\log \hat{\boldsymbol{s}}$ (element-wise) and that the trivial solution $\hat{\boldsymbol{s}} = \boldsymbol{0}$ is not assumed. We solve this problem using a solver implemented in `scipy.optimize.least_squares`.

E Experimental Details

In this section, we provide details on the experimental setups. We provide the full source-code for the experimental evaluation in a ZIP file along with this submission to enhance reproducibility. We fully commit to open-sourcing our code in case of acceptance.

E.1 Fitting transformers on a synthetic dataset

E.1.1 Dataset construction

We create a synthetic dataset to ensure a linear relationship between features and log-odds. Before sampling the dataset, we fix a vocabulary of tokens, ground truth scores for each token, and their occurrence probability.

Algorithm 1 Local efficient SLALOM approximation (SLALOM-`eff`)

Require: Sequence $\boldsymbol{t}$, trained model F (outputs log odds), random sample length n, learning rate λ, batch size r, sample pool size b, number of steps c
Initialize $v(t_i) = 0$, $s(t_i) = 0 \ \ \forall$ unique $t_i \in \boldsymbol{t}$
$B \leftarrow b$ samples of random sequences of length n obtained through uniform sampling of unique tokens in $\boldsymbol{t}$.
Precompute $F(B[i]), i = 1, \ldots, b$ *# perform model forward-pass for each sample in pool*
steps $\leftarrow 0$
while steps $< c$ **do**
$B' \leftarrow$ minibatch of r samples uniformly sampled from the sample pool B
loss $\leftarrow \frac{1}{r}\sum_{k=1}^{r}\left(F(B'[k]) - \text{SLALOM}_{v,s}(B'[k])\right)^2$ *# compute MSE btw. F and SLALOM using precomputed models outputs* $F(B')$
$v \leftarrow v - \lambda \nabla_v \text{loss}$ *# Back-propagate loss to update SLALOM parameters*
$s \leftarrow s - \lambda \nabla_s \text{loss}$
steps $\leftarrow$ steps $+ 1$
end while
return v, $s - \text{mean}(s)$ *# normalize s to zero-mean*

Algorithm 2 Local high-fidelity SLALOM approximation (SLALOM-`fidel`)

Require: Sequence $\boldsymbol{t}$, trained model F (outputs log odds), max. number of deletions n, learning rate λ, batch size r, sample pool size b, number of steps c
Initialize $\boldsymbol{s} = 0$, $\boldsymbol{s} = 0 \ \ \forall$ unique $t_i \in \boldsymbol{t}$
$B \leftarrow b$ samples of random sequences of length n obtained through deleting up to n tokens randomly from $\boldsymbol{t}$.
Precompute $F(B[i]), i = 1, \ldots, b$ *# perform model forward-pass for each sample in pool*
steps $\leftarrow 0$
while steps $< c$ **do**
$\boldsymbol{v} = \arg\min_{\boldsymbol{v}'} \sum_{i=1}^{b}\left(F(B[i]) - \text{SLALOM}_{\boldsymbol{v}',\boldsymbol{s}}(B[i])\right)^2$ *# Fix* $\boldsymbol{s}$ *and optimize* $\boldsymbol{v}$*, OLS problem*
$\boldsymbol{s} = \arg\min_{\boldsymbol{s}'} \sum_{i=1}^{b}\left(F(B[i]) - \text{SLALOM}_{\boldsymbol{v},\boldsymbol{s}'}(B[i])\right)^2$ *# Fix* $\boldsymbol{v}$ *and optimize* $\boldsymbol{s}$*, Quadratic problem*
steps $\leftarrow$ steps $+ 1$
end while
return $\boldsymbol{v}$, $\boldsymbol{s} - \text{mean}(\boldsymbol{s})$ *# normalize s to zero-mean*

This means that each of the possible tokens already comes with a ground-truth score w that has been manually assigned. The tokens, their respective scores w, and occurrence probabilities are listed in Table 3. Samples of the dataset are sampled in four steps that are exectued repeatedly for each sample:

1. A sequence length $|\boldsymbol{t}| \sim \text{Bin}(p = 0.5, n{=}30)$ is binomially distributed with an expected value of 15 tokens and a maximum of 30 tokens
2. We sample $|\boldsymbol{t}|$ tokens independently from the vocabulary according to their occurrence probability (Table 3)
3. Third, having obtained the input sequence, we can evaluate the linear model by summing up the scores of the individual tokens in a sequence:

$$F(\boldsymbol{t}) = F([t_1, t_2, \ldots, t_{|\boldsymbol{t}|}]) = \sum_{i=1}^{|\boldsymbol{t}|} w(t_i). \tag{80}$$

4. Having obtained the log-odds ratio for this sample F(t), we sample the labels according to this ratio. We have $p(y = 1)/p(y = 0) = \exp(F(\boldsymbol{t}))$, which can be rearranged to $p(y = 1) = \frac{\exp(F(\boldsymbol{t}))}{1+\exp(F(\boldsymbol{t}))}$. We sample a binary label y for each sample according to this probability.

The tokens appear independently with the probability $p_{\text{occurrence}}$ given in the table.

word	"the"	"we"	"movie"	"watch"	"good"	"best"	"perfect"	"ok"	"bad"	"worst"
linear weight w	0.0	0.0	0.0	0.0	0.6	1.0	1.5	-0.6	-1.0	-1.5
$p_{\text{occurrence}}$	1/6	1/6	1/6	1/6	1/15	1/20	1/20	1/15	1/20	1/20

Table 3: Tokens in the linear dataset with their corresponding weight

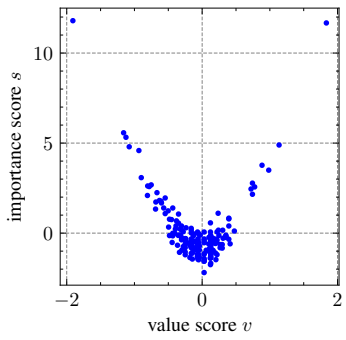

Figure 8: Score distribution for the tokens for the analytical SLALOM used in the recovery experiment.

E.1.2 Post-hoc fitting of surrogate models

We train the models on this dataset for 5 epochs, where one epoch contains 5000 samples at batch size of 20 using default parameters otherwise.

For the results in Figure 3, we query the models with sequences that contain growing numbers of the work perfect, i.e. ["perfect", "perfect", ...]. We prepend a CLS token for the BERT models.

For the results in Figure 4, we then sample 10000 new samples from this dataset (having the same distribution as the training samples) and forward them through the trained transformers. The model log-odds score together with the feature vectors are used to train the different surrogate models, linear model, GAM, and SLALOM. For the linear model, we fit an OLS on the log-odds returned by the model. We use the word counts for each of the 10 tokens as a feature vector. The GAM provides the possibility to assign each token a different weight according to its position in the sequence. To this end, we use a different feature vector of length $30 \cdot 10$. Each feature corresponds to a token and a position and is set to one if the token i is present at this position, and set to 0 otherwise. We then fit a linear model using regularized (LASSO) least squares with a small regularization constant of $\lambda = 0.01$ because the system is numerically unstable in its unregularized form.

E.2 Recovering SLALOMs from observations

We resort to a second synthetic dataset to study the recovery property for the SLALOM. To find a realistic distribution of scores, we compute a BoW importance scores for input tokens of the BERT model on the IMDB dataset by counting the class-wise occurrence probabilities. We select 200 tokens randomly from this dataset. We use these scores as value scores v but multiply them by a factors of 2 as many words have very small BoW importances. In realistic datasets, we observed that value scores v are correlated with the importance scores s. Therefore, we sample

$$s(\tau) \sim 5\left(v(\tau)^{\frac{3}{2}}\right) + \frac{1}{2}\mathcal{N}(0,1)\,, \tag{81}$$

which results in the value/importance distribution given in Figure 8. We assign each word an equal occurrence probability and sample sequences of words at uniformly distributed lengths in random $[1, 30]$. After a sequence is sampled, labels are subsequently sampled according to the log-odds ratio of the SLALOM. We train the transformer models on $20 \cdot 20000$ samples. When using a smaller vocabulary size, we only sample the sequences out of the first $|\mathcal{V}|$ possible tokens.

dataset	DistilBERT	BERT	GPT-2
IMDB	0.88	0.90	0.74
Yelp	0.86	0.88	0.88

Table 4: **Accuracies of models used in this paper.** For IMDB ($|trainset| = 5000$), we use 2-layer versions of the models. For Yelp, ($|trainset| = 5000$), we use 6-layer versions of the models. For both datasets, the $|testset| = 100$. The models are trained for 2 epochs after which we found the accuracy of the model on the test set to have converged.

E.3 Training Details for real-World data experiments

Training details. In these experiments, we use the IMDB (Maas et al., 2011) and Yelp (Asghar, 2016) datasets to train transformer models on. Specifically, the results in Table 1a are obtained by training 2-layer versions of BERT, DistilBERT and GPT-2 with on 5000 samples from the IMDB dataset for 2 epoch, respectively. We did not observe significant variation in terms of number of layers, so we stick to the simpler models for the final experiments. For the experiments in Table 1b we train and use 6-layer versions of the above models for 2 epochs on 5000 samples of the Yelp dataset. We report the accuracies of these models in Table 4 and additional hyperparameters in Table 5.

SLALOM vs. Naïve Bayes Ground Truth. To arrive at the Spearman rank-correlations between SLALOM importance scores s, value scores v and their combination ($\exp(s) \cdot v$) with a ground truth, we fit SLALOM on each of the trained models and use a Naïve-Bayes model for ground truth scores. The model is given as follows:

$$\log \frac{p(y=1|\boldsymbol{t})}{p(y=0|\boldsymbol{t})} = \log \frac{p(y=1)}{p(y=0)} + \sum_{t_i \in \boldsymbol{t}} \log \frac{p(t_i|y=1)}{p(t_i|y=0)} \tag{82}$$

We obtain $\frac{p(t_i|y=1)}{p(t_i|y=0)}$ by counting class-wise word frequencies, such that we obtain a linear score w for each token τ given by $w(\tau) = \frac{(\#\text{occ. of } \tau \text{ in class } 1)+\alpha}{(\#\text{occ. of } \tau \text{ in class } 0)+\alpha}$. We use Laplace smoothing with $\alpha = 40$. The final correlations are computed over a set of 50 random samples, where we observe good agreement between the Naïve Bayes scores, and the value and linearized SLALOM scores, respectively. Note that the importance scores are considered unsigned, such that we compute their correlation with the absolute value of the Naive Bayes scores.

SLALOM vs. Human Attention. The Yelp Human Attention (HAT) (Sen et al., 2020) dataset consists of samples from the original Yelp review dataset, where for each review real human annotators have been asked to select the words they deem important for the underlying class (i.e. positive or negative). This results in binary attention vectors, where each word either is or is not important according to the annotators. Since each sample is processed by multiple annotators, we use the consensus attention map as defined in Sen et al. (2020), requiring agreement between annotators for a token to be considered important to aggregate them into one attention vector per sample. Since HAT, unlike SLALOM, operates on a word level, we map each word's human attention to each of its tokens (according to the employed model's specific tokenizer).
To compare SLALOM scores with human attention in Table 1b, we choose the AU-ROC metric, where the binary human attention serves as the correct class, and the SLALOM scores as the prediction. We observe how especially the importance scores of SLALOM are reasonably powerful in predicting human attention. Note that the human attention scores are unsigned, such that we also use absolute values for the SLALOM value scores and the linearized version of the SLALOM scores for the HAT prediction.

F Additional Experimental Results

F.1 Fitting SLALOM as a Surrogate to Transformer outputs

We provide an additional emprical counterexample for why GAMs cannot describe the transformer output in Figure 9. The example provides additional intuition for why the GAM is insufficient to describe transformers acting like a *weighted* sum of token importances.

parameter	value
learning rate	5e-5
batch size	5
epochs	2
dataset size used	5000
number of heads	12
number of layers	2 (IMDB), 6 (Yelp)
num. parameter	31M - 124M

(a) Hyperparameters

specification	value
CPU core:	AMD EPYC 7763
Num. CPU cores	64-Core (128 threads)
GPU type used	1xNvidia A100
GPU-RAM	80GB
Compute-Hours	$\approx$ 150 h

(b) Hardware used (internal cluster)

Table 5: Overview over relevant hyperparameters and hardware

architecture	L (num.layers)	linear model	GAM	SLALOM
GPT-2	1	20.31 ± 2.02	48.78 ± 2.70	**16.92** ± 1.33
GPT-2	2	24.81 ± 3.11	54.33 ± 3.26	**22.17** ± 1.98
GPT-2	6	32.66 ± 7.60	57.08 ± 7.19	**21.59** ± 4.14
GPT-2	12	25.74 ± 4.18	54.36 ± 3.94	**20.25** ± 2.37
DistilBERT	1	28.28 ± 4.30	44.43 ± 2.22	**10.83** ± 2.13
DistilBERT	2	32.58 ± 7.75	53.87 ± 7.20	**16.82** ± 4.38
DistilBERT	6	31.49 ± 4.06	49.35 ± 3.13	**17.26** ± 3.64
DistilBERT	12	50.82 ± 9.21	71.64 ± 9.19	**27.50** ± 4.18
BERT	1	26.33 ± 1.90	43.30 ± 0.88	**7.34** ± 0.70
BERT	2	28.43 ± 3.75	48.28 ± 3.23	**9.92** ± 1.19
BERT	6	50.82 ± 6.34	68.23 ± 4.59	**23.99** ± 3.38
BERT	12	44.58 ± 13.15	51.38 ± 14.71	**18.77** ± 6.78

Table 6: MSE ($\times$100) when fitting SLALOM to the outputs of transformer models trained on the linear dataset. SLALOM manages to describe the outputs of the transformer significantly better than other surrogate models *even if the underlying relation in the data was linear.*

We report Mean-Squared Errors when fitting SLALOM to transformer models trained on the linear dataset in Table 6. These results underline that SLALOM outperforms linear and additive models when fitting them to the transformer outputs. Note that even if the original relation in the data was linear, the transformer does not represent this relation such that the SLALOM describes its output better. We present additional qualitative results for other models in Figure 10 that support the same conclusion.

F.2 Fitting SLALOM on Transformers trained on data following the SLALOM distribution

We report Mean-Squared Errors in the logit-space and the parameter-space between original SLALOM scores and recovered scores. The logit output are evaluated on a test set of 200 samples that are sampled from the original SLALOM. We provide these quantitative results in Table 7 for logit scores the result are very small Table 8. In logits the differences are negligibly small, and seem to decrease further with more layers. This finding highlight that a) transformers with more layers still easily fit SLALOMs and such model can be recovered in parameters space. The results on the MSE in parameter space show no clear trend, but are relatively small as well (with the largest value being MSE=0.015 (note that results in the table are multiplied by a factor of 100 for readability). Together with our quantitative results in Figure 4(c,d), this highlights that SLALOM has effective recovery properties.

Input Sequence	BERT score	GAM weight assignments	SLALOM weight assignments
perfect	**2.5**	Assign w_1("perfect") = 2.5	Assign v("perfect") = 2.5
perfect perfect	**2.5**	Assign w_2("perfect") = 0	Expected SLALOM output: 2.5
worst	**-2.6**	Assign w_1("worst") = −2.6	Assign v("worst") = −2.6
worst worst	**-2.5**	Assign w_2("worst") = 0.1	Expected SLALOM output: -2.6
worst perfect	**0.0**	↯ Expected GAM output w_1("perfect") + w_2("worst") = 2.6	Assign s("perfect") = s("worst") = 0 Expected SLALOM output: -0.05

Figure 9: A simple empirical counterexample for why GANs cannot describe transformer output. We report rounded scores by a real 4-layer BERT model (similar behavior was observed for other layers/architectures) and iteratively fit the GAM $F(\boldsymbol{t}) = \sum_{t_i \in \boldsymbol{t}} w_i(t_i)$ to match observed outputs on the two tokens "perfect" and "worst". We quickly arrive at a contradiction for the GAM. On the contrary, we can assign SLALOM scores that model this behavior with minor error. Because transformers behave like a weighted sum of importances, GAMs are insufficient to model their behavior. In conjunction with Figure 4(a,b) this underlines that GAMs and linear models are insufficient as surrogates.

L (num.layers)	DistilBERT	BERT	GPT-2
1	0.002 ± 0.001	0.002 ± 0.000	0.011 ± 0.009
2	0.003 ± 0.002	0.003 ± 0.002	0.017 ± 0.011
6	0.001 ± 0.001	0.011 ± 0.007	<0.001 ± 0.000
12	<0.001 ± 0.000	<0.001 ± 0.000	<0.001 ± 0.000

Table 7: MSE (×100), logit space, averaged over 5 runs

L (num.layers)	DistilBERT	BERT	GPT-2
1	0.092 ± 0.045	0.540 ± 0.301	0.940 ± 0.392
2	0.094 ± 0.049	0.368 ± 0.085	1.652 ± 0.903
6	0.124 ± 0.030	0.830 ± 0.182	0.569 ± 0.177
12	0.287 ± 0.088	0.394 ± 0.255	0.385 ± 0.126

Table 8: MSE (×100), parameter space, averaged over 5 runs

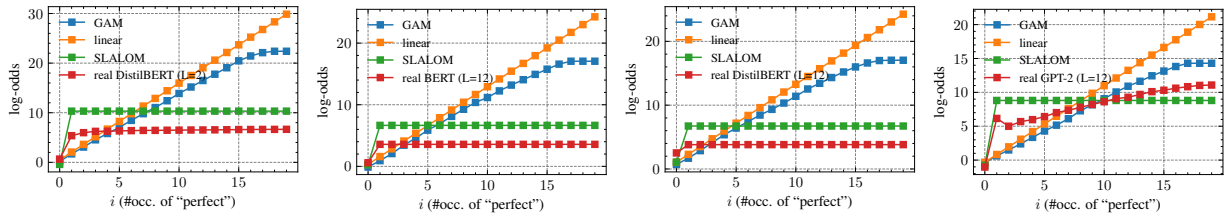

(a) DistilBERT (L=2) (b) BERT (L=12) (c) DistilBERT (L=12) (d) GPT-2 (L=12)

Figure 10: **SLALOM describes outputs of transformer models well.** Fitting SLALOM to the outputs of the models shown in Figure 3 using the synthetic dataset. We show results for a sequence containing repetitions of the token "perfect". Note however that the models were trained on a larger dataset of random sequences samples as described in Appendix E.1.1, but these sequences were chosen for visualization purposes. Results on additional models. Despite having $C/2{=}15\times$ more parameters than the SLALOM model, the GAM model does not describe the output as accurately. We provide quantitative results in Table 6.

F.3 Additional Results on Real-World Data

We obtain SLALOM explanations for real-world data using the procedure outlined in Algorithm 1 (SLALOM-`eff`) with sequences of length $n = 2$ and with Algorithm 2 (SLALOM-`fidel`) removing up to 5 tokens that we compare with Naive-Bayes scores and Human Attention.

F.3.1 Additional Qualitative Results

Figure 12 shows the full results from the sample used in Figure 5, where we only visualized a choice of words for readability purposes. After running SLALOM-`eff` on our trained IMDB models, we use to explain a movie review taken from the dataset, visualizing value scores v against importance scores s.

F.3.2 Correlation with Naive-Bayes Scores

We compare the scores obtained with SLALOM with the scores obtained with other methods in Table 9, obtaining scores that are reliable with SLALOM-`eff` (value scores and linear scores) in particular. While SHAP achieves higher correlation on BERT, SLALOM achieves higher correlation than LIME and SHAP on all models and higher correlations than LRP for GPT-2 while obtaining slightly inferior values for the BERT-based architectures.

F.3.3 Human Attention

In Figure 11, we show qualitative results for a sample from the Yelp-HAT dataset. After fitting SLALOM on top of the resulting model, we can extract the importance scores given to each token in the sample. We can see that the SLALOM scores manage to identify many of the tokens which real human annotators also deemed important for this review to be classified as positive. We also show qualitative results for the other methods. However, we suggest caution when interpreting explanations visually without ground truth. We argue that (1) theoretical properties of explanations (2) comparing to a known ground truth as well as (3) consideration of metrics from different domains, e.g., faithfulness, human perspective, are required to allow for a comprehensive evaluation. This is the approach taken in our work.

We show a quantitative comparison of the scores obtained with SLALOM with the scores obtained with other methods on the comparison with Human-Attention in Table 10.

F.4 Insertion and Removal Benchmarks

It is important to verify that SLALOM scores are competitive to other methods in classical explanation benchmarks as well. We therefore ran the classical removal and insertion benchmarks with SLALOM compared to baselines such as LIME, SHAP, Grad (Simonyan et al., 2013), and Integrated Gradients (IG,

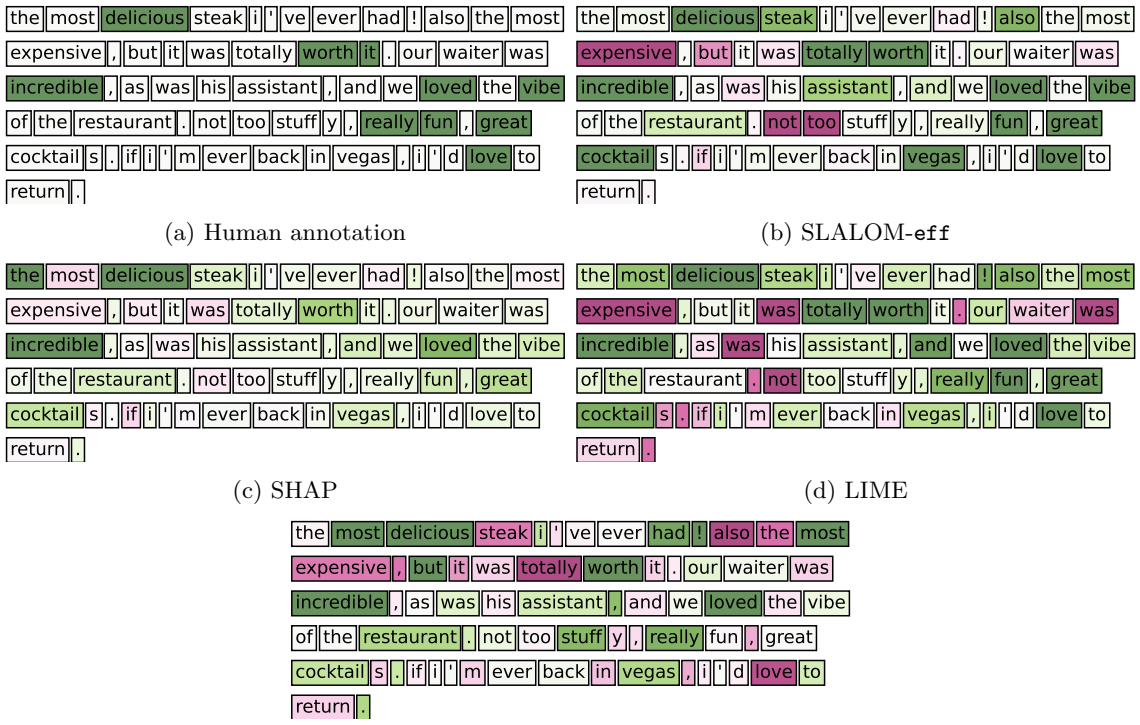

(a) Human annotation

(b) SLALOM-`eff`

(c) SHAP

(d) LIME

(e) AttnLRP

Figure 11: **Qualitative comparisons of attribution maps.** We provide attribution maps for the different techniques in this figure. Many words deemed important by human annotators are likewise highlighted by SLALOM and other techniques.

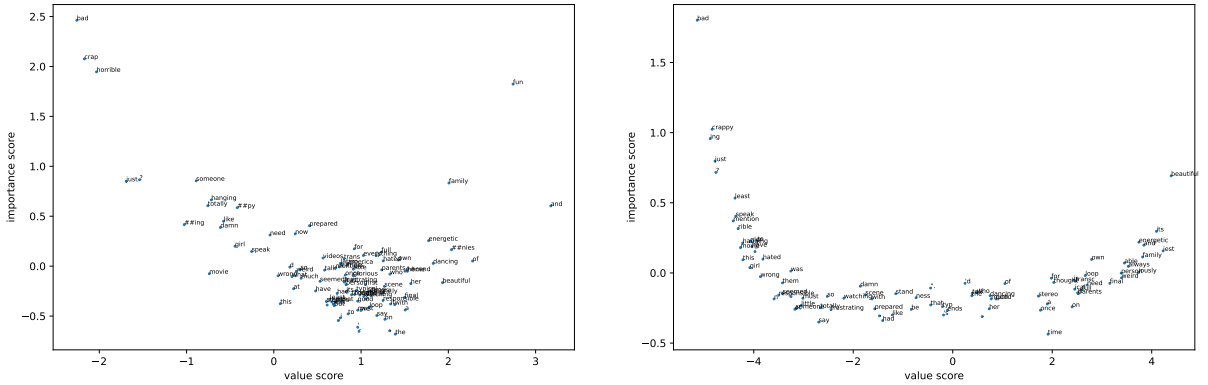

(a) BERT

(b) GPT-2

Figure 12: Full scatter plots of SLALOM scores for the sample shown in the main paper (please zoom in for details). We observe that words like “bad” or “fun” get assigned high importance scores and value scores of high magnitude (albeit with different signs) by SLALOM.

	SLALOM-`fidel`			SLALOM-`eff`		
LM	values v	importances s	lin. SLALOM	values v	importances s	lin. SLALOM
DistilBERT	0.602 ± 0.10	0.020 ± 0.08	0.602 ± 0.10	0.692 ± 0.05	0.373 ± 0.09	0.693 ± 0.05
BERT	0.475 ± 0.12	0.031 ± 0.09	0.474 ± 0.12	0.619 ± 0.08	0.349 ± 0.09	0.626 ± 0.08
GPT-2	0.467 ± 0.17	0.017 ± 0.08	0.468 ± 0.17	0.618 ± 0.08	0.292 ± 0.10	0.619 ± 0.08

LM	LIME	SHAP	IG	Grad	LRP
Distilbert	0.691 ± 0.05	0.619 ± 0.06	-0.285 ± 0.12	-0.215 ± 0.12	0.706 ± 0.05
BERT	0.616 ± 0.08	0.554 ± 0.09	-0.125 ± 0.14	-0.123 ± 0.14	0.639 ± 0.08
GPT2	0.213 ± 0.13	0.560 ± 0.09	0.033 ± 0.13	0.031 ± 0.13	0.615 ± 0.08

Table 9: Correlation with linear Naive Bayes Scores. The scores obtained with SLALOM-`eff` (value, lin.) are better than those from LIME, SHAP and comparable to LRP scores.

LM	values v	importances s	lin.	LIME	SHAP	LRP
Bert	0.786 ± 0.01	0.807 ± 0.01	0.801 ± 0.01	0.805 ± 0.01	0.800 ± 0.01	0.813 ± 0.01
Distil-BERT	0.688 ± 0.01	0.681 ± 0.01	0.686 ± 0.01	0.702 ± 0.01	0.668 ± 0.01	0.703 ± 0.01
GPT-2	0.674 ± 0.01	0.685 ± 0.01	0.683 ± 0.01	0.632 ± 0.01	0.671 ± 0.01	0.699 ± 0.01

Table 10: Comparison of techniques to predict Human Attention. SLALOM-eff (importances) perform better than SHAP, comparably to LIME and slightly below LRP.

Sundararajan et al., 2017). For the insertion benchmarks, the tokens with the highest attributions are inserted to quickly obtain a high prediction score to the target class. For the deletion benchmark, the tokens with the highest attributions are deleted from the sample to obtain a low score for the target class. We subsequently delete/insert more tokens and compute the "Area Over the Perturbation Curve" (AOPC) as in DeYoung et al. (2020), which should be high for deletion and low for insertion. In addition to the insertion results in Table 1c, the removal results are shown in Table 11a. We show results for the Yelp dataset in Table 11b and Table 11c. Our linear SLALOM scores perform par with LIME and SHAP in this benchmark. For surrogate techniques (LIME, SHAP, SLALOM) we use 5000 samples each.

F.5 Error Analysis for non-transformer models

We also investigate the behavior of SLALOM for models that do not precisely follow the architecture described in the Analysis section of this paper. In the present work, we consider an attribution method that is specifically catered towards the transformer architecture, which is the most prevalent in sequence classification. We advise caution when using our model when the type of underlying LM is unknown. In this case, model-agnostic interpretability methods may be preferred.

However, we investigate this issue further: We applied our SLALOM-`eff` approach to a simple, non-transformer sequence classification model on the IMDB dataset, which is a three-layer feed-forward network based on a TF-IDF representation of the inputs. We compute the insertion and deletion Area-over-perturbation-curve metrics that are given in Table 12.

These results show that due to its general expressivity, the SLALOM model also succeeds to provide explanations for non-transformer models that outperform LIME and SHAP in the removal and insertion tests. We also invite the reader to confer Table 15 and Appendix F.7, where we show that SLALOM can predict human attention for large models, including the non-transformer Mamba model (Gu & Dao, 2023).

F.6 Runtime analysis

We ran SLALOM as well as other feature attribution methods using surrogate models and compared their runtime to explain a single classification of a 6-layer BERT model. We note that the runtime is mainly determined by the number of forward passes to obtain the samples to fit the surrogates. While this number is independent of the dataset size, longer sequences require more samples for the same approximation quality. The results are shown in Table 13.

	SLALOM-fidel		SLALOM-eff						
LM	v-scores	lin.	v-scores	lin.	LIME	SHAP	IG	Grad	LRP
BERT	0.893 ± 0.012	0.901 ± 0.012	0.881 ± 0.010	0.885 ± 0.010	0.875 ± 0.012	0.881 ± 0.011	0.084 ± 0.010	0.069 ± 0.008	0.852 ± 0.019
DistilBERT	0.841 ± 0.014	0.854 ± 0.013	0.888 ± 0.008	0.886 ± 0.008	0.838 ± 0.012	0.864 ± 0.009	0.143 ± 0.012	0.131 ± 0.012	0.865 ± 0.011
GPT-2	0.837 ± 0.013	0.844 ± 0.013	0.782 ± 0.013	0.784 ± 0.012	0.479 ± 0.024	0.859 ± 0.012	0.289 ± 0.021	0.269 ± 0.020	0.833 ± 0.013
average	0.857 ± 0.013	0.866 ± 0.013	0.851 ± 0.010	0.852 ± 0.010	0.731 ± 0.016	0.868 ± 0.011	0.172 ± 0.014	0.156 ± 0.013	0.850 ± 0.014

(a) IMDB: Area-Over Perturbation Curve (deletion, higher is better)

	SLALOM-fidel		SLALOM-eff						
LM	v-scores	lin.	v-scores	lin.	LIME	SHAP	IG	Grad	LRP
BERT	0.015 ± 0.005	0.011 ± 0.005	0.011 ± 0.005	0.011 ± 0.005	0.017 ± 0.009	0.012 ± 0.005	0.224 ± 0.024	0.214 ± 0.022	0.010 ± 0.005
DistilBERT	0.018 ± 0.006	0.019 ± 0.006	0.032 ± 0.009	0.032 ± 0.009	0.014 ± 0.005	0.020 ± 0.005	0.250 ± 0.027	0.249 ± 0.026	0.017 ± 0.009
GPT-2	0.033 ± 0.007	0.032 ± 0.007	0.045 ± 0.007	0.045 ± 0.007	0.129 ± 0.019	0.021 ± 0.004	0.251 ± 0.024	0.244 ± 0.024	0.039 ± 0.007
average	0.022 ± 0.006	0.021 ± 0.006	0.029 ± 0.007	0.029 ± 0.007	0.053 ± 0.011	0.018 ± 0.005	0.242 ± 0.025	0.236 ± 0.024	0.022 ± 0.007

(b) Yelp: Area-Over Perturbation Curve (insertion, lower is better)

	SLALOM-fidel		SLALOM-eff						
LM	v-scores	lin.	v-scores	lin.	LIME	SHAP	IG	Grad	LRP
GPT-2	0.747 ± 0.024	0.753 ± 0.024	0.726 ± 0.021	0.727 ± 0.021	0.444 ± 0.028	0.849 ± 0.015	0.292 ± 0.026	0.290 ± 0.026	0.740 ± 0.025
BERT	0.657 ± 0.038	0.667 ± 0.038	0.865 ± 0.012	0.863 ± 0.013	0.797 ± 0.022	0.859 ± 0.013	0.249 ± 0.028	0.281 ± 0.029	0.855 ± 0.017
DistilBERT	0.645 ± 0.033	0.642 ± 0.033	0.813 ± 0.017	0.813 ± 0.018	0.746 ± 0.025	0.854 ± 0.013	0.201 ± 0.026	0.243 ± 0.028	0.768 ± 0.024
average	0.683 ± 0.032	0.687 ± 0.032	0.801 ± 0.017	0.801 ± 0.017	0.663 ± 0.025	0.854 ± 0.014	0.247 ± 0.027	0.271 ± 0.028	0.788 ± 0.022

(c) Yelp: Area-Over Perturbation Curve (deletion, higher is better)

Table 11: Additional results for removal/insertion tests: We show results on the IMDB dataset for removal as well as insertion and removal on the Yelp datset.

	SHAP	LIME	lin. SLALOM-eff
Insertion (lower)	0.0120 ± 0.005	0.0053 ± 0.003	0.0039 ± 0.001
Deletion (higher)	0.8022 ± 0.026	0.9481 ± 0.005	0.9601 ± 0.004

Table 12: AOPC explantion fidelity metrics for the Fully Connected TF-IDF model. The scores highlight that SLALOM can also provide faithful explanations for non-transformer models due to its general expressivity.

While IG and Gradient explanations are the quickest, they also require backward passes which have large memory requirements. As expected, the computational complexity for surrogate model explanation (LIME, SHAP, SLALOM) is dominated by the number of samples and forward passes done. **Our implementation of SLALOM is around 2x faster than LIME and almost 5x faster than SHAP** (all approaches used a GPU-based, batching-enabled implementation), which we attribute to the fact that SLALOM can be fitted using substantially shorter sequences than are used by LIME and SHAP.

We are interested to find out how many samples are required to obtain an explanation of comparable quality to SHAP. We successively increase the number of samples used to fit our surrogates and report the performance in the deletion benchmark (where the prediction should drop quickly when removing the most important tokens). We report the Area over the Perturbation Curve (AOPC) as before (this corresponds to their Comprehensiveness metric of ERASER (DeYoung et al., 2020), higher scores are better). We compare the performance to `shap.KernelExplainer.shap_values(nsamples=auto)` method of the shap package in Table 14. Our results indicate that sampling sizes as low as 500 per explained instance (which is as low as predicted by our theory, with average sequence length of 200) already yields competitive results.

F.7 Applying SLALOM to Large Language Models

Our work is mainly concerned with sequence classification. In this application, we observe mid-sized models like BERT to be prevalent. On the huggingface hub, among the 10 most downloaded models on huggingface, 9

(a) DistilBERT

Approach / # samples	1000	2000	5000	10000
SHAP	2.35 ± 0.01	4.62 ± 0.02	11.56 ± 0.03	23.08 ± 0.08
LIME	0.80 ± 0.04	1.58 ± 0.07	3.93 ± 0.19	8.04 ± 0.39
SLALOM-`fidel`	0.74 ± 0.03	1.42 ± 0.06	3.77 ± 0.24	7.95 ± 0.41
SLALOM-`eff`	0.42 ± 0.01	0.80 ± 0.01	2.03 ± 0.01	4.13 ± 0.02
LRP	0.02 ± 0.00	0.02 ± 0.00	0.02 ± 0.00	0.02 ± 0.00
IG	0.02 ± 0.00	0.02 ± 0.00	0.02 ± 0.00	0.02 ± 0.00
Grad	0.01 ± 0.00	0.01 ± 0.00	0.01 ± 0.00	0.01 ± 0.00

(b) BLOOM-7B

Runtime (s)	SHAP	LIME	IG	Grad	SLALOM-`eff`
1000 Samples	25.04 ± 2.37	15.73 ± 2.37	0.29 ± 0.04	0.06 ± 0.01	0.62 ± 0.02

Table 13: Runtime results for computing different explanations. SLALOM is substantially more efficient that other surrogate model explanations (e.g., LIME, SHAP). Gradient-based explanations can be computed even quicker, but are very noisy and require backward passes. Runtimes are given in seconds (s).

Number of samples	Deletion AOPC
SHAP (nsamples="auto")	0.9135 ± 0.0105
SLALOM, 500 samples	0.9243 ± 0.0105
SLALOM, 1000 samples	0.9236 ± 0.005
SLALOM 2000 samples	0.9348 ± 0.005
SLALOM, 5000 samples	0.9387 ± 0.005
SLALOM, 10000 samples	0.9387 ± 0.005

Table 14: Ablation study on the number of samples required to obtain good explanations. The results highlight that a number as low as 500 samples can be sufficient to fit the surrogate model at a quality comparable to SHAP.

LM	values v	importances s	lin. $(\exp(s) \cdot v)$
BLOOM-7B	0.69 ± 0.01	**0.71** ± 0.02	0.70 ± 0.02
Mamba-2.8B	0.69 ± 0.02	0.32 ± 0.02	**0.70** ± 0.01

Table 15: ROC-Scores for predicting Human attention with SLALOM-`eff` using LLMs

are BERT-based and the remaining one is another transformer with around 33M parameters[3] (as of September 2023). In common benchmarks like DBPedia classification[4], the top-three models are transformers with two of them also being variants of BERT. We chose our experimental setup to reflect this. Nevertheless, we are interested to see if SLALOM can provide useful insights for larger models as well and therefore experiment with larger models. To this end, we use a model from the BLOOM family (Le Scao et al., 2023) with 7.1B parameters as well as the recent Mamba model (2.8B) (Gu & Dao, 2023) on the Yelp-HAT dataset and compute SLALOM explanations. Note that the Mamba model does not even follow the transformer framework considered in this work. We otherwise follow the setup described in Figure 3 and assess whether our explanations can predict human attention. The results in Table 15 highlight that this is indeed the case, even for larger models. The ROC scores are in a range comparable to the ones obtained for the smaller models. For the non-transformer Mamba model we observe a drop in the value of the importance scores. This may suggest that value scores and linearized SLALOM scores are more reliable for large, non-transformer models.

[3] `https://huggingface.co/models?pipeline_tag=text-classification&sort=downloads`
[4] `https://paperswithcode.com/sota/text-classification-on-dbpedia`